Edge Preservation in Nonlinear Diffusion Filtering

Mohammad Reza Hajiaboli

A Thesis
in
The Department
of
Electrical and Computer Engineering

Presented in Partial Fulfillment of the Requirements
for the Degree of Doctor of Philosophy at
Concordia University
Montréal, Québec, Canada

March 2012

CONCORDIA UNIVERSITY
SCHOOL OF GRADUATE STUDIES

This is to certify that the thesis prepared

By: Mohammad Reza Hajiaboli

Entitled: Edge Preservation in Nonlinear Diffusion Filtering

and submitted in partial fulfilment of the requirements for the degree of

DOCTOR OF PHILOSOPHY (Electrical & Computer Engineering)

complies with the regulations of the University and meets the accepted standards with respect to originality and quality.

Signed by the final examining committee:

Dr. A.K.W. Ahmed _____ Chair

_____ External Examiner
Dr. M.A. Bayoumi

_____ External to Program
Dr. T. Fancott

_____ Examiner
Dr. M.N.S. Swamy

_____ Examiner
Dr. W-P. Zhu

_____ Co-Supervisor
Dr. M.O. Ahmad

_____ Co-Supervisor
Dr. C. Wang

Approved by _____
Dr. J.X. Zhang, Graduate Program Director

April 13 2012

Dr. Robin A.L. Drew, Dean
Faculty of Engineering & Computer Science

ABSTRACT

Edge Preservation in Nonlinear Diffusion Filtering

Mohammad Reza Hajiaboli, Ph.D.
Concordia University, 2012

Image denoising techniques, in which the process of noise diffusion is modeled as a nonlinear partial differential equation, are well known for providing low-complexity solutions to the denoising problem with a minimal amount of image artifacts. In discrete settings of these nonlinear models, the objective of providing a good noise removal while preserving the image edges is heavily dependent on the kernels, diffusion functions and the associated contrast parameters employed by these nonlinear diffusion techniques. This thesis makes an in-depth study of the roles of the kernels and contrast parameters with a view to providing an effective solution to the problem of denoising of the images contaminated with stationary and signal-dependent noise.

Within the above unified theme, this thesis has two major parts. In the first part of this study, the impact of anisotropic behavior of the Laplacian operator on the capabilities of nonlinear diffusion filters in preserving the image edges in different orientations is investigated. Based on this study, an analytical scheme is devised to obtain a spatially-varying kernel that adapt itself to the diffusivity function. The proposed edge-adaptive Laplacian kernel is then incorporated into various nonlinear diffusion filters for denoising of images contaminated by additive white Gaussian noise.

The performance optimality of the the existing nonlinear diffusion techniques is generally based on the assumption that the noise and signal are uncorrelated. However, in many applications, such as in medical imaging systems and in remote sensing where the images are degraded by Poisson noise, this assumption is not valid. As such, in the second part of the thesis, a study is undertaken for denoising of images contaminated by Poisson noise within the framework of the Perona-Malik nonlinear

diffusion filter. Specifically, starting from a Skellam distribution model of the gradient of the Poisson-noise corrupted images and following the diffusion mechanism of the nonlinear filter, a spatially and temporally varying contrast parameter is designed. It is shown that the nonlinear diffusion filters employing the new Laplacian kernel supports the extremum principle and that the proposed contrast parameter satisfies the sufficient conditions for observance of the scale-space properties.

Extensive experiments are performed throughout the thesis to demonstrate the effectiveness and validity of the various schemes and techniques developed in this investigation. The simulation results of applying the new Laplacian kernel to a number of nonlinear diffusion filters show its distinctive advantages over the conventional Rosenfeld and Kak kernel, in terms of the filters' noise reduction and edge preservation capabilities for images corrupted by additive white Gaussian noise. The simulation results of incorporating the proposed spatially- and temporally-varying contrast parameter into the Perona-Malik nonlinear diffusion filter demonstrate a performance much superior to that provided by some of the other state-of-the-art techniques in denoising images corrupted by Poisson noise.

To my lovely wife, Shaghayegh

ACKNOWLEDGEMENTS

The support of my supervisors Professor M. Omair Ahmad and Professor Chunyan Wang during the development of this research is gratefully acknowledged.

TABLE OF CONTENTS

LIST OF FIGURES

LIST OF TABLES

LIST OF SYMBOLS

$c(.)$	Commonly used diffusivity function
d	Orthogonal directions in two-dimensional spatial domain
f^*	Noiseless image
f	Noisy image
f_M^*	Maximum gray level of the noiseless image
$g(.)$	Diffusivity function in the form of Perona and Malik
I	Noiseless image
$I_\alpha(.)$	Modified Bessel function of the first kind
K	Contrast parameter
L_1	Laplacian Kernels
L_2	Laplacian Kernels
$L_{i,j}$	Spatially varying Laplacian kernel
(n)	Iteration number
$\mathcal{P}(\mu)$	Poisson distribution with parameter μ
$\Pr(.)$	Probability density function
$\mathcal{S}(.,.)$	Skellam distribution
u	Diffusing image
u_{max}	Maximum gray level of the diffusing image
u_{min}	Minimum gray level of the diffusing image
$u_x,\ u_y,\ u_t$	Derivative of u with respect of x, y, t respectively
$u_{\xi\xi}$	Second-order derivative of u in the direction of the level sets
$u_{\eta\eta}$	Second-order derivative of u in the direction of the gradient
σ^2	Variance
σ	Standard deviation
$\phi(.)$	Flux function

τ	Time step-size
$\|.\|$	Euclidean norm
$\|.\|$	Absolute value
∇u	Gradient of u
$\nabla_d u$	Gradient in the direction d
$\nabla^2 u$	Laplacian of u

LIST OF ACRONYMS

AWGN	Additive white Gaussian noise
CCD	Charged-coupled device
DCT	Discrete cosine transform
FOM	Pratt's figure of merit
FT	Fourier Transform
GVF	Gradient vector flow
ICA	Independent component analysis
KL	Kullback-Leibler
MCM	Mean curvature motion
MRI	Magnetic resonance imaging
MSD	Mean squared difference
PDE	Partial differential equation
PDF	Probability distribution function
PSNR	Peak signal-to-noise ratio
SAR	Satellite aperture radar
SNR	Signal-to-noise ratio
SIW	Shift invariance wavelet transform
TIW	Translation invariance wavelet transform
TV	Total variation
UDWT	Undecimated wavelet transform

Chapter 1

Introduction

1.1 Digital Image Denoising

Image processing is a rapidly growing field of research because of its widespread applications in military, commercial, entertainment, medical and many other sectors of the society. Technological advances in digital imaging, computer processors and mass storage devices have fueled this growth. Image processing tasks that in the past have employed analog systems in their implementation are now being implemented using digital systems because of the flexibility and affordability provided by the latter.

The field of image processing is concerned primarily with extracting useful information from images. Image processing algorithms may be classified in three different categories. In the first category, there are techniques that carry out low-level processing using directly the raw pixels, with denoising and edge detection being good examples of such techniques. In the second category, there are algorithms that utilize the results of the low-level processing for other types of processing, such as segmentation, classification and edge linking. In the third category of digital image processing algorithms, there are techniques that attempt to extract semantic meaning from the

information provided by the algorithms in the first and second categories. For example, pattern recognition or object tracking algorithms belong to this category.

In digital imaging systems, noise from various sources contaminates the acquired image and hinders the performance of the image processing algorithms. Thus, denoising of the acquired image that improves the signal-to-noise ratio (SNR) is needed prior to applying any higher-level image processing algorithms.

Noise is defined to be an uncertainty or imprecision with which a signal is recorded [1]. One type of noise that is produced by a typical charge-coupled device (CCD) image sensor is an additive white Gaussian noise (AWGN) with zero mean [2]. In many imaging systems such as those used in medical, astronomical and remote sensing applications, images are acquired in a low-illumination condition and, therefore, referred to as photon-limited images. In such a situation, the image is degraded mainly by a Poisson noise [3]. The Poisson noise has strong signal dependency [4, 5].

A denoised image is an approximation of the underlying true image prior to becoming contaminated by the noise. A variety of denoising filtering techniques have been introduced in the literatures [6–8]. However, there is always a trade-off between the smoothing efficiency of a denoising technique, preservation of discontinuity and generation of artifacts in the resulting denoised image. In the following, some of the well-known noise filtering techniques are briefly reviewed.

1.2 A Brief Review of Noise Filtering Techniques

Image denoising schemes can be classified to two broad categories, linear and nonlinear techniques. In linear denoising techniques, the denoised images are obtained by performing some averaging operation on the image pixels in the spatial domain or first by transforming the image in the frequency domain and then performing certain low-pass filtering operations on the transformed image. There are number of transform

domain filtering techniques that employ discrete transform, such as Fourier transform (FT) [9], cosine transform [10], Haar transform [11], and wavelet transform [12–15]. These transform-domain techniques make use of the fact that the coefficients of the transformed image are decorrelated into low and high frequency components. The problem with these techniques, however, is that since the edges also belong to high frequency regions, the filtering process, while denoising the image, results in distorting the edges. The trade-off between the noise removal and edge preservation in these techniques is generally controlled by a suitable choice of cut-off/threshold frequency of the filters. Wavelet-based linear techniques for image denoising offer significant advantages over other frequency domain filters, such as different choices in selecting basis functions and spatial frequency tiling [16]. However, these techniques have limitations [17]: (i) The specific distributions of the signal and noise may not be well matched at different scales. (ii) The choice of the threshold, which is the most important design parameter, is made in an ad hoc manner.

To address the disadvantages of the linear denoising techniques, nonlinear filters have been developed which are computationally more intensive, but they provide better edge-preservation. In the context of wavelet-based denoising, based on formal Bayesian theory, Simoncelli et al. [18] have developed nonlinear estimators for detecting the threshold parameter that outperform its linear counterparts. They used a generalized Laplacian model for the subband statistics of the image and developed a noise-removal algorithm, which performs a "coring" operation to the data. This same idea has also been followed by other researchers to develop other wavelet-based denoising methods based on different statistical models for subband wavelet coefficients. For instance, in [19], a generalized Gaussian probability distribution function (PDF) has been used to model the subband wavelet coefficients, and in [20–22] a Gauss-Hermite PDF to model the empirical wavelet coefficients. Other examples of spatially-adaptive techniques for thresholding wavelet coefficients to remove noise from medical and

satellite aperture radar (SAR) images can be found in [23–27]. However, the use of the orthogonal wavelet transform in these denoising techniques results in artifacts in the denoised images due to the pseudo-Gibbs phenomena [11], which arise from the fact that the orthogonal wavelet transforms are not shift-invariant and thus, the singularities at different locations are represented differently in these transforms [28]. To reduce the impact of pseudo-Gibbs phenomena, the undecimated wavelet transform (UDWT) has been introduced. This transform has been independently proposed under several names, e.g., translation invariant wavelet transform (TIW) [29], shift invariant wavelet transform (SIW) [30], and stationary wavelet transform (SWT) [31]. In the case of the orthogonal wavelet transforms, the wavelet coefficients of the signal and those associated with the noise are uncorrelated. However, in the case of UDWT, this property does not hold, since it is a non-orthogonal transform [32].

A class of nonlinear filters is median filters [33, 34] in which each pixel value in the denoised image is the median of a set of the noisy pixels in a small window of the image. The performance of these filters depends on the size of the image window but the filters fail to provide a good visual performance for images highly contaminated by noise [11]. Another class of nonlinear filters is the partial differential equation (PDE) based filters [35, 36]. These filter are well known for their good edge preservation capabilities without producing ringing artifacts. These filtering schemes have been widely used in medical image denoising [37, 37–43], where it is of paramount of importance that the denoising process preserves the information contained in high-spatial-frequency components of the images. However, when the level of the contaminating noise is moderate or high, these filters fail to provide a good balance between noise reduction and edge preservation in the denoised image and pin-hole artifacts in the denoised image are formed [44, 45].

The performance optimality of denoising techniques in terms of their edge preservation and noise removal capabilities is generally based on the assumption that the

noise and signal are uncorrelated and contaminating noise is stationary such as AWGN. However, the assumption of stationarity and additivity do not hold for cases in which images are acquired under low illumination condition such as cases in medical imaging or remote sensing systems. In these cases, the images are degraded mainly by Poisson noise. For removing Poisson noise, which is a non-stationary and signal correlated noise, some methods have been developed, which belong to the category of nonlinear denoising filters. One of the techniques to denoise images corrupted by Poisson noise is to first apply the nonlinear Anscombe transform [46] or its simpler form, the square root transform [47], in order to reduce the correlation between the signal and the noise, and then use any denoising technique, developed based on the assumption of uncorrelated noise, to process the transformed image. Some other techniques that are more effective in removing Poisson noise have also been developed. The wavelet-based denoising [48–53] is one category of such techniques. However, the denoised images obtained by these techniques have ringing artifacts around the edges. The formation of these artifacts can somewhat be reduced by incorporating the external cycle-spinning mechanism [54] in the wavelet filtering at the expense of an increased computational complexity.

A variational filter has also been introduced for removing Poisson noise, which can be seen as an approach for minimizing a cost function consisting of two terms, a term representing the total variation (TV) of the regularized image [36] and a fidelity term representing the Kullback-Liebler (KL) divergence between the regularized and noisy images [55]. Due to the non-smoothness of the cost function and the non-quadratic and non-separable nature of its KL divergence term, many different approximate methods have been proposed to solve this nonlinear problem [56–61]. The quality of the denoised images provided by the filters is highly dependent on the effectiveness of the numerical solver used for the solution of the minimization problem.

1.3 Motivation

The nonlinear diffusion filters are powerful denoising techniques in view of their superior edge preservation capability without producing ringing artifacts in the filtered images. These filters perform time evolutionary processes, in which the denoised image is a solution of a diffusion equation modeled as a PDE with spatially varying diffusion coefficients. Since the introduction of the first nonlinear diffusion filter by Perona and Malik [35] in 1990, enhancing the performance of the PDE-based nonlinear diffusion further has been a subject of many research efforts [44, 45, 62–66]. In these improved techniques, the focus has been on introducing new or modified diffusivity functions providing better control of the diffusion process.

Digital realization of PDE, modeling the nonlinear diffusion process, invariably makes use of kernels to approximate time and spatial rate of change of the image intensities. It should be noted that the kernels themselves have impact on the characteristics of the diffusing images. This impact of the kernels needs to be studied in the context of noise removal and edge preservation capabilities of the nonlinear diffusion process.

In nonlinear diffusion filters, a diffusivity function is used to control the diffusion process. In order to provide a good control of the noise diffusion and edge preservation, such a function should be a function of image gradient as well as image intensities. Most of the diffusivity functions are chosen to be a function of image gradient and a contrast parameter. With a proper choice of this parameter, the rate of diffusion at edge pixels are made different from that at non-edge pixels. In most cases, a spatially constant value of this parameter is judiciously chosen so as to provide a good balance between edge preservation and noise removal. Some limited studies for obtaining the spatially varying contrast parameter have been made and that too only for the cases where images are contaminated by additive white Gaussian noise. Little effort seems to have been made to carry out a comprehensive study on the impact of the contrast

parameter in diffusing the noise and preserving the edges of images, specially when the images are contaminated by other kinds of noise.

1.4 Scope of the Thesis

This thesis is concerned with the development of PDE-based techniques for removing the noise in images. The focus of the research is on studying the impact of the kernels and contrast parameters in removing the noise of the images while preserving their edges.

In the first part of the thesis, a study is undertaken to investigate the impact of the anisotropic behavior of the Laplacian operator of nonlinear diffusion filters. Based on this study, an edge-adaptive Laplacian kernel is designed with a view to providing filters with a better edge preservation capability while removing the noise effectively.

In the second part of the thesis, a systematic study is conducted for understanding the mechanism of image diffusion from the view point of the choice of the contrast parameter used by a nonlinear diffusion filter. Through this study, a spatially and temporally varying contrast parameter is evolved within the framework of the Perona-Malik nonlinear diffusion filter with an objective of preserving the edges while effectively denoising the images corrupted by Poisson noise.

1.5 Organization of the Dissertation

The dissertation is organized as follows.

In Chapter 2, a brief account of the development of the Perona-Malik nonlinear diffusion filter is given. The development begins with a premise that image diffusion is a process satisfying the scale-space properties and ends with a nonlinear PDE

model for the process of image diffusion. A couple of discrete models of the Perona-Malik filter, each emphasizing on a different strategy for noise diffusion and edge preservation, is discussed. This chapter serves as a background material necessary for the development of the work undertaken in this thesis.

In Chapter 3, the effect of the anisotropic behavior of Rosenfeld and Kak's Laplacian kernel on the edge preservation capability of a discretized version of the Perona and Malik's nonlinear diffusion filter is first studied. Based on this study, an edge-adaptive Laplacian kernel, which exploits this anisotropic behavior in providing a more effective edge preservation capability, is developed. The new kernel is incorporated into the Perona-Malik filter as well as into some other nonlinear diffusion filters to demonstrate its effectiveness in enhancing their capability in providing better performance.

In Chapter 4, the role of contrast parameters in denoising images contaminated by Poisson noise is investigated. Starting from a Skellam distribution model of the image gradient and carrying out a systematic analysis of the diffusion process of the Perona-Malik nonlinear filter, a spatially and temporally varying contrast parameter is designed. The scale-space properties of the Perona-Malik filter incorporating this contrast parameter is also examined. Finally, in this chapter, the effectiveness of the newly designed contrast parameter is experimentally investigated and performance of the filter compared with that of other state-of-the-art nonlinear filters.

Finally, Chapter 5, summarizes the work of the study undertaken in this thesis and highlights its contributions. Some suggestions for further work based on the ideas and schemes developed in this thesis are also given.

Chapter 2

Background Material

2.1 Nonlinear Diffusion Denoising

The Gaussian scale-space [67] can be considered a striating point of diffusion based image processing techniques. The Gaussian scale-space is derived by convolving the original image $u_0(x, y)$ with a Gaussian kernel $G(x, y, t)$ of variance $\sigma^2 = t$, where t is an artificial time index. The resulting linear scale-space for $t : 0 \longmapsto +\infty$ is a family of derived images in form of

$$u(x, y, t) = u_0(x, y) * G(x, y, t) \tag{2.1}$$

where $u(x, y, t)$ has coarser resolution as t marching to infinity. Later, Koenderink [68] and Hummel [69] have shown that the convolution of u_0 with Gaussian kernel with variance of t is equivalent to the solution of standard heat conduction equation in form of

$$\frac{\partial u(x, y)}{\partial t} = \nabla^2 u(x, y) \tag{2.2}$$

at $t = \sigma^2/2$ with the initial condition $u(x, y, 0) = u_0(x, y)$, where ∇^2 denotes the Laplacian operation. This linear diffusion equation (2.2) can be used for removing

the noise from the initial image u_0; however, the diffusion rate of the noise and edges are equal; thus, the edges on image will be eliminated, displaced or blurred. A major breakthrough to this problem has been proposed by Perona and Malik in [35], where they introduced the nonlinear diffusion equation given by

$$\partial u/\partial t = div\left(c\left(\|\nabla u\|\right)\nabla u\right) \quad \text{on} \quad \Omega \times (0, +\infty), \tag{2.3}$$

subject to the boundary and initial conditions

$$\begin{aligned} \partial u/\partial n = 0 \quad &\text{on} \quad \partial\Omega \times (0, +\infty)\,, \\ u(x, y, 0) = f \quad &\text{on} \quad \Omega\,, \end{aligned}$$

where f is a noisy image, $\partial u/\partial n$ is the derivative of the image on the normal to the image boundary $\partial\Omega$, $\|.\|$ and div denote the $L_2 - norm$ and divergence respectively and $c(.)$ is the diffusivity function also referred to as the diffusion coefficients. For notational simplicity, $u(x, y, t)$ is denoted as u. The diffusivity function is a positive, and non-increasing function of $\|\nabla u\|$ and two of these diffusivity functions introduced in [35] are

$$c\left(\|\nabla u\|\right) = K^2/\left(K^2 + \|\nabla u\|^2\right) \tag{2.4}$$

and

$$c\left(\|\nabla u\|\right) = \exp - \left(\frac{1}{2}\left(\frac{\|\nabla u\|}{K}\right)^2\right), \tag{2.5}$$

where K is a positive parameter called a contrast parameter. The value of the parameter K is chosen such that the diffusion coefficient, $c\left(\|\nabla u\|\right)$, is close to one for regions of u with $\|\nabla u\| \ll K$, whereas it is close to zero for $\|\nabla u\| \gg K$, which leads to a good edge preservation by reducing the diffusivity for the high contrast edges. The nonlinear diffusion (2.3) can be seen as a minimization problem of a potential cost function (see e.g. [70, 71]) in from of

$$min\left\{\int_\Omega \rho(s)dxdy\right\}, \tag{2.6}$$

where $s = \|\nabla u\|$ and $\rho(s)$ is a function associated with a diffusivity function as

$$\rho(s) = \int \phi(s)ds = \int sc(s)ds \ , \tag{2.7}$$

where $\phi(s)$ is called the flux function. Using the diffusivity functions of Perona and Malik, the associated potential function is non-convex leading to ill-posedness of (2.3). In this case, edges and noise with $s > K$ are facing an inverse diffusion (i.e. the enhancement). To overcome the difficulty arose from the ill-posedness of the nonlinear diffusion process one of the possibility is to use the a different diffusivity function by which the flux function of $\varphi(s) = \rho'(s)$ is monolithically increasing with respect to s, i.e., $d(\phi(s))/ds \ > 0$. An example of these diffusivity functions is introduced by Charbunnier [72] in the form of

$$c\left(\|\nabla u\|\right) = \left(K^2/\left(K^2 + \|\nabla u\|^2\right)\right)^{-1/2} \ . \tag{2.8}$$

Another practical approach for increasing the stability of the nonlinear diffusion process, when the associated potential function is of non-convex, is to employ the spatial regularization scheme introduced by Catte et al. [73]. In this scheme, the diffusivity function is replaced by $c\left(\|\nabla\left(u * G_\sigma\right)\|\right)$ where u is convolved by a Gaussian kernel, G_σ, with a standard deviation of σ.

In general, using the diffusivity function by which the associated potential function becomes non-convex or even concave is more desirable for increasing the edge preservation capability of the filter. In this regard, different diffusivity functions have been introduced such as the ones by Wieckert [64] and Gilboa *et al.* [74] with a non-convex potential function, and Keeling and Stollberger's function [63] by which the potential function is concave.

The main question that for while in literature has been refer to as *Perona-Malik Paradox* [66] is that the nonlinear diffusion using the diffusivity functions for which the associated potential function is non-convex should lead to instability. However, the results does not show any instability. The research in [64] has shown that the

nonlinear diffusion filter that is discretized in spatial domain in particular way can be seen as well-posed diffusion process which can support the associated scale-space properties. Two of commonly used discretized model of the nonlinear diffusion filter are provided in Section 2.2.

Apart from the variety in diffusivity functions, the nonlinear diffusion equation itself has been formulated in different ways. One of early models emerged from the expansion of the divergence in (2.3) by Alvarez et al. [75] is in the form of

$$u_t = c\left(\|\nabla u\|\right) u_{\xi\xi} + \left(c\left(\|\nabla u\|\right) + c'\left(\|\nabla u\|\right)\|\nabla u\|\right) u_{\eta\eta} \quad , \tag{2.9}$$

where $u_{\xi\xi}$ and $u_{\eta\eta}$ are the second derivative of u in the direction of the level sets (i.e., the direction parallel to the image features) and the direction of the gradient (i.e., the direction across the edge). Knowing that *c(.)* is a positive coefficient, (2.9) can be interpreted as a combination of a forward diffusion term in the direction of the level set and a term that could possibility perform the backward diffusion process in the direction of the gradient since $\left(c\left(\|\nabla u\|\right) + c'\left(\|\nabla u\|\right)\|\nabla u\|\right)$ can be negative.

A class of nonlinear diffusion filters known as anisotropic diffusion filters has been developed in which the diffusion rate is spatially controlled based on the direction of the local features. Using the directional dependent smoothing for image enhancement can be traced back to the work of [76]. However, in context of PDE-based filters for image processing, we can refer to the method of [77] known as mean curvature motion (MCM) as one of the earliest method in which the smoothing is performed only in the direction of level sets. Based on the idea of MCM, other nonlinear filters have been developed such as the ones introduced by [78] and [79] for image denoising and segmentation.

Among the other directional dependent smoothing filters (i.e., anisotropic) filters, we can refer to the model of [64, 80] in both edge and coherence-enhancing formulations, or the model of [81] and its improved one [82] developed for denoising of vector-valued images.

Starting from (2.9), Carmona and Zhong [83] introduced a more generalized PDE for the nonlinear diffusion filter in the form of

$$u_t = a\left(\|\nabla u\|\right)\left(b\left(\|\nabla u\|\right)u_{\xi\xi} + c\left(\|\nabla u\|\right)u_{\eta\eta}\right) \ , \tag{2.10}$$

where the diffusivity function $a(.)$ controls the total diffusion and the diffusivity functions of $b(.)$ and $c(.)$ control the diffusivity in the direction of the level sets and gradient.

2.2 Numerical Solution

A commonly used numerical model for the Perona-Malik filter [35] is based on an explicit forward Euler approximation of $\partial u/\partial t$ in the time and using the 4-nearest neighborhood pixels in direction of x and y in the space. This numerical model for each pixel of a digital image, u, with a constant grid size of $\Delta x = \Delta y = 1$ at position of (i, j) is given by

$$u_{i,j}^{(n+1)} = u_{i,j}^{(n)} + \tau\left[c_N\nabla_N u + c_S\nabla_S u + c_E\nabla_E u + c_W\nabla_W u\right]_{i,j}^{(n)} , \tag{2.11}$$

where n is the number of iterations, τ is a time step-size for approximation of $\partial u/\partial t$ and for stability reason, it is bounded in range of *(0, 0.25]*. The evolved image u^n is usually considered as diffused image at a virtual time of $t = \tau \times n$. Directional gradients of u for any pixel at position of *(i,j)* are given by

$$\begin{aligned} \nabla_N u_{i,j} &= u_{i+1,j} - u_{i,j} \ , \quad & \nabla_S u_{i,j} &= u_{i-1,j} - u_{i,j} \ , \\ \nabla_E u_{i,j} &= u_{i,j+1} - u_{i,j} \ , \quad & \nabla_W u_{i,j} &= u_{i,j-1} - u_{i,j} \ , \end{aligned} \tag{2.12}$$

which are the result of subtraction of each pixel value from the pixel values of the 4-nearest neighbors in the directions of north (N), south (S), east (E) and west (W). The diffusion coefficients of c_N, c_S, c_E and c_W are updated at every iteration as a

function of the gradient in the form of

$$c_N = c\left(\|\nabla u_{i+1/2,j}\|\right) \ , \quad c_S = c\left(\|\nabla u_{i-1/2,j}\|\right) \ ,$$
$$c_E = c\left(\|\nabla u_{i,j+1/2}\|\right) \ , \quad c_W = c\left(\|\nabla u_{i,j-1/2}\|\right) \ . \tag{2.13}$$

For approximation of the diffusion coefficients at the arc locations, one of the simple and crude choice as Perona and Malik have suggested, is to approximate the norm of gradient at each arc location with the absolute value of its projection along the direction of the arc [35], which leads to

$$c_d \approx c\left(|\nabla_d u|\right) \ , \text{where } d \in \{N, S, E, W\} \ . \tag{2.14}$$

Approximation of c_d as as an arithmetic average of the diffusivity at the adjacent nodes has also been suggested [65, 84] in the form of

$$c_N \approx \left(c\left(\|\nabla u_{i+1,j}\|\right) + c\left(\|\nabla u_{i,j}\|\right)\right)/2 \ ,$$
$$c_S \approx \left(c\left(\|\nabla u_{i-1,j}\|\right) + c\left(\|\nabla u_{i,j}\|\right)\right)/2 \ ,$$
$$c_E \approx \left(c\left(\|\nabla u_{i,j+1}\|\right) + c\left(\|\nabla u_{i,j}\|\right)\right)/2 \ ,$$
$$c_W \approx \left(c\left(\|\nabla u_{i,j-1}\|\right) + c\left(\|\nabla u_{i,j}\|\right)\right)/2 \ . \tag{2.15}$$

It is important to note that $\sum_d \nabla_d u$ is equal to Laplacian of u, $\nabla^2 u$. To calculate $\nabla^2 u$, a discrete Laplacian Kernel of L_1 in the from of

$$L_1 = \begin{bmatrix} 0 & 1 & 0 \\ 1 & -4 & 1 \\ 0 & 1 & 0 \end{bmatrix}$$

is convolved by u. Therefore, by substituting (2.15) in (2.11) and after adding and subtracting of $\left(c\left(\|\nabla u_{i,j}\|\right)\nabla^2 u\right)/2$ and simplifications, one can derive the following numerical model

$$u_{i,j}^{(n+1)} = u_{i,j}^{(n)} + \tau \left[\sum_{d\in D} c\nabla^2 u + \frac{\tau}{2}\left[\nabla_d c \nabla_d u\right]\right]_{i,j}^{(n)} \ , \quad D = \{N, S, E, W\} \tag{2.16}$$

where ∇_d denotes the directional gradient based on (2.12) for both function $c(.)$ and u.

In the numerical model of (2.16), the second term at the right side is a nonlinear forward diffusion term and the third term can lead to an inverse diffusion which results in the formation of the staircases of the ramp edges. Some advantages of (2.16) compared to (2.11) have been mentioned in [85] and [86] such as flexibility of the adjustment of the forward and inverse diffusion rate.

Other spatial discretization of the Perona-Malik filter also have been introduced such as [63, 87] by incorporating the different neighborhood pixels rather than those in orthogonal directions. For spatial discretization of the expanded models of the nonlinear diffusion filters given by (2.9) and (2.10), the spatial partial derivative are usually approximated by central difference operators.

2.3 Summary

In this chapter, the background material necessary for the development of the research undertaken in this thesis has been presented. A brief account of the development of the PDE-based nonlinear diffusion filter of Perona and Malik has been given. The effect of diffusivity functions and the role they play in preserving edges have been discussed. Finally, two commonly used discretized versions of the Perona-Malik nonlinear diffusion filter have also been presented.

Chapter 3

An Edge-Adaptive Laplacian Kernel for Nonlinear Diffusion Filters

3.1 Introduction

In this chapter, the Laplacian kernel is investigated from the point of view of its impact on edge preservation capability in nonlinear diffusion of images. A technique based on the anisotropic behavior of the Rosenfeld and Kak Laplacian operator [88] is presented for an efficient preservation of the edges in nonlinear diffusion processes [89]. A study is undertaken first to investigate the impact of the anisotropic behavior of the Laplacian operator on the capability of nonlinear diffusion filters in preserving edges in different orientations and then to explore the possibility of designing a new Laplacian operator that is best suited to preserve the edges in certain orientations without affecting the quality of the edges in other directions. It is shown that the coefficients of the kernel can be is derived so as to integrate into it an anisotropic behavior to control the process of forward diffusion in horizontal and vertical directions. Even though the proposed constant-coefficient kernel reduces the process of edge distortion,

it nonetheless produces artifacts in the smooth regions of the image. After examining the source of this problem, an analytical scheme is devised to obtain an edge-adaptive Laplacian kernel that adapt itself to the diffusivity function. The proposed Laplacian kernel is then used in various nonlinear diffusion filters starting from the classical Perona-Malik filter to the more recent ones. The effectiveness of the new kernel, using quantitative and qualitative measures, is demonstrated by applying it to images contaminated by additive white Gaussian noise (AWGN).

3.2 Impact of the Anisotropic Behavior of the Laplacian Operator on the Diffusion Rate of Edges

The basic nonlinear diffusion filter of Perona and Malik [35], characterized by a nonlinear partial differential equation, is given by

$$\partial u/\partial t = div\left(c\left(\|\nabla u\|\right)\nabla u\right) \ , \tag{3.1}$$

where $\|.\|$ and div denote, respectively, the L_2-norm and divergence of the associated quantities, *c(.)* is a diffusivity function, also referred to as the diffusion coefficients, and ∇u represent the gradient of the diffusing image u. By carrying out the divergence operation with respect to the independent variable x and y of u, the above equation can be expressed as follows:

$$\partial u/\partial t = c(.)\nabla^2 u + \nabla c(.)\nabla u \tag{3.2}$$

in which $\nabla^2 u$ denotes the Laplacian of u. A commonly used discrete version [65, 84] of (3.1) (or equivalently of (3.2)) in which the diffusivity function is approximated by the arithmetic average of the diffusivity coefficients at the adjacent nodes, is given by

$$u_{i,j}^{(n+1)} = u_{i,j}^{(n)} + \tau\left[c_{i,j}\nabla^2 u_{i,j}\right]^{(n)} + \frac{\tau}{2}\left[\sum_d \nabla_d c_{i,j}\nabla_d u_{i,j}\right]^{(n)} , \tag{3.3}$$

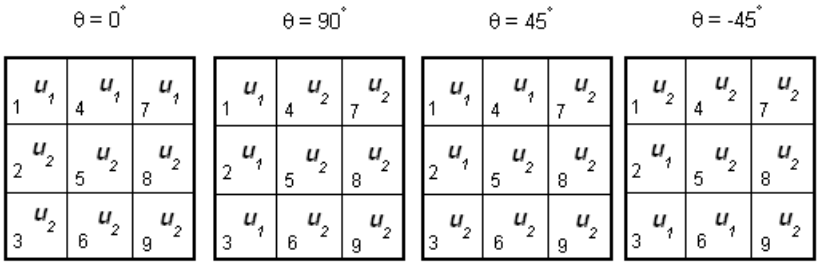

Figure 3.1: Four step edges with the same contrast level of $(u_1 - u_2)$ and orientations of $\theta = 0°, 90°, 45°, -45°$.

where ∇_d , $d \in \{N, S, E, W\}$, denotes the directional gradient calculated as the difference of two adjacent pixel values or diffusion coefficients in the north (N), south (S), east (E) and west (W) directions, τ is the step-size of the independent variable t used for the approximation of $\partial u/\partial t$, and n is the discrete time index (or the iteration number). The Laplacian $\nabla^2 u$ in the approximation given by (3.3) is actually the discrete convolution of u with the so-called Rosenfeld-Kak Laplacian kernel L_1 [88]) given by

$$L_1 = \begin{bmatrix} 0 & 1 & 0 \\ 1 & -4 & 1 \\ 0 & 1 & 0 \end{bmatrix} .$$

The Laplacian kernel L_1 has an anisotropic response to step edges [90] in the sense that the convolution result of the constant-contrast edge is orientation dependent. To show this anisotropic response, one can consider four step edges with the same contrast level of $(u_1 - u_2)$ and orientations of θ, as shown in 3.1

If the central pixel of these intensity functions is denoted by I_5, the Laplacian responses of I_5 for the four orientation values is given by

$$\begin{array}{cccccc} & \theta = 90\,° & \theta = 0\,° & \theta = +45\,° & \theta = -45\,° \\ \nabla^2 I_5 = & (u_1 - u_2) & (u_1 - u_2) & 2(u_1 - u_2) & 2(u_1 - u_2) \; . \end{array}$$

This simple example shows that the response of L_1 to an edge in horizontal or vertical direction is different from that to the diagonal edge thus confirming the anisotropic behavior of the discrete Laplacian operator.

We now focus our attention to study the impact of the anisotropic behavior of the Laplacian operator L_1 on the performance of the discrete nonlinear diffusion filters, in as far as their capability in preserving edges.

In (3.3), the values $c(\|\nabla u\|)$, calculated based on central difference operator for $\|\nabla u\|$, on both sides of a step edge are the same; thus, the directional derivative of $\nabla_d c(.)$ is zero. Therefore, at step edges, the nonlinear diffusion equation given in (3.3) becomes

$$u_{i,j}^{(n+1)} = u_{i,j}^{(n)} + \tau \left[c_{i,j} \nabla^2 u_{i,j}\right]^{(n)} . \tag{3.4}$$

In fact, the same simplification achieved from the nonlinear diffusion equation of Alvarez et al. [75] given by

$$u_t = c\left(\|\nabla u\|\right) u_{\xi\xi} + \left(c\left(\|\nabla u\|\right) + c'\left(\|\nabla u\|\right) \|\nabla u\|\right) u_{\eta\eta} \ , \tag{3.5}$$

where $u_{\xi\xi}$ and $u_{\eta\eta}$ are the second-order derivatives of u in the direction of the level set (i.e. the direction parallel to the image features) and the direction of the gradient (i.e. the direction across the edge). In this case, $\nabla^2 u = u_{\eta\eta} + u_{\xi\xi}$ and for step edges $u_{\xi\xi} = 0$, this nonlinear diffusion filter at the step edges in the continuous domain assumes the form

$$u_t = c(\|\nabla u\|)\nabla^2 u \ , \tag{3.6}$$

which can be seen to have the same discrete version as the one given by (3.4).

Equation (3.4) governs the diffusion process at edges has another difference operator arising from the diffusion coefficient *c(.)*, which also has an anisotropic behavior. In order to study the impact of only the anisotropic behavior of the Laplacian operator (i.e. L_1) on the diffusion process of the edges, we use the Scharr kernels [91] to have the rotationally invariant (isotropic) approximation of $\|\nabla u\|$.

Two synthetic digital images shown in 3.2(a) and (b) containing vertical and a diagonal edge, respectively, are chosen. The contrast level of the edge in both images is 70 thus the variance of either images is approximately 1225. These two images

are filtered in accordance with the diffusion process of (3.4) in which the diffusivity function of Perona and Malik given by

$$c\left(\|\nabla u\|\right) = K^2 / \left(K^2 + \|\nabla u\|^2\right) \ , \tag{3.7}$$

where K is a positive parameter called a contrast parameter, is used. The value of K, which is manually set, controlls the the diffusion in the sense that the larger value of K results in a more intense diffusion. The diffusion process is repeated by varying the values of K from 5 to 25 in steps of 0.5. For each run, τ is chosen as 0.1 and the diffusion process stopped after $n = 30$ iterations. The variance of the diffused image is calculated. The result of the variance of the diffused image as a function of K is plotted in Figure 3.2(c). It is seen from this figure that the image containing the vertical edge is less diffused than the one with the diagonal edge. Thus, the same diffusion precess can preserve a vertical edge better than a diagonal one.

It is important to note that the commonly used approximation of $\|\nabla u\|$ is based on the central difference operator [45], which is an anisotropic operator. In our experiment, by using this operator to calculate the diffusivity function and L_1 for the Laplacian operator, we obtain results that are also depicted in Figure 3.2(c). As seen from this figure, an isotropic or anisotropic approximation of $\|\nabla u\|$ has a little or no impact on the diffusion of the edges. However, the results of Figure 3.2(c) also indicates that there are significant differences between the diffusions of the vertical and diagonal edges. This observation motivates us to develop a new kernel with the capability of providing a better control of the diffusion of edges.

3.3 Proposed Laplacian Kernel

Our objective in this section is to explore the possibility of designing a Laplacian kernel from the standpoint of reducing the diffusion process of the edges and make the process less dependent on their orientation of the edges. Hence, in the context of

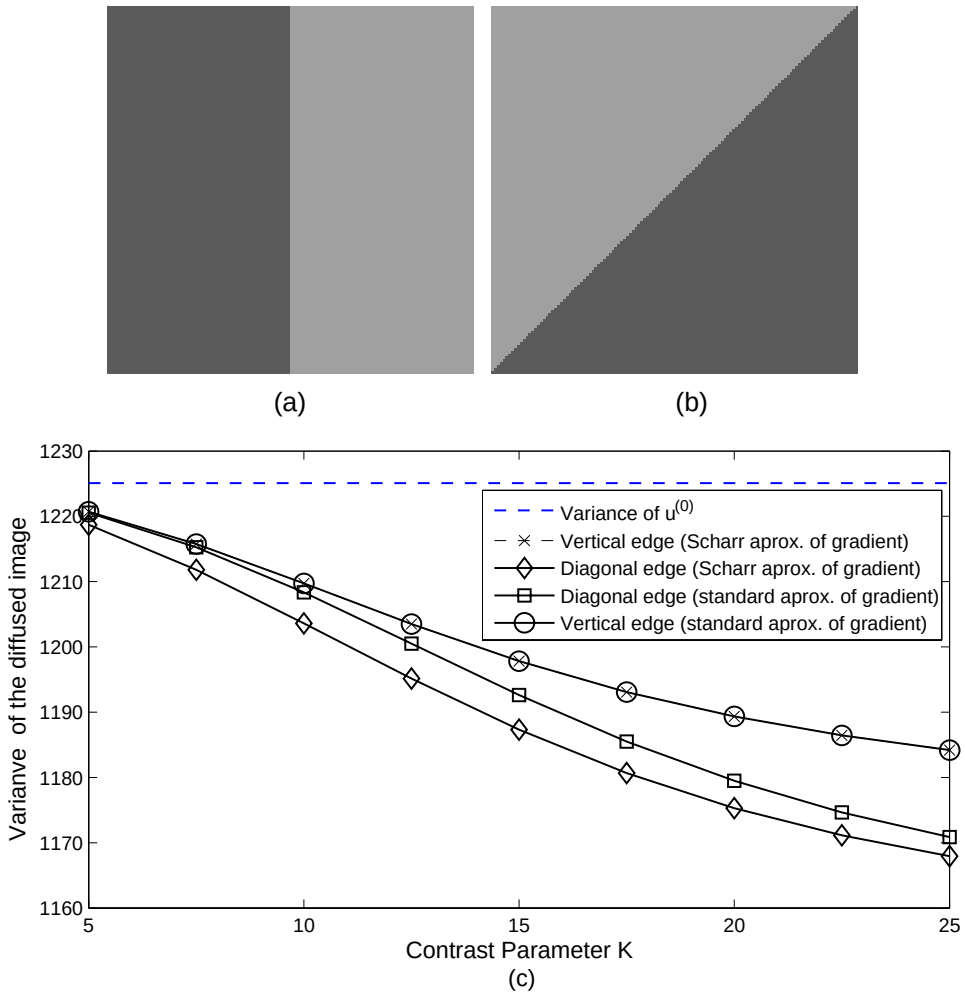

Figure 3.2: Impact of the anisotropic behavior of the L_1 kernel, when used in (3.3), on the vertical and diagonal edges. (a) Image with a vertical edges. (b) Image with a diagonal edge. (c) Variance of the diffused images using isotropic and anisotropic discrete approximations of $\|\nabla u\|$.

Figure 3.2(c), our objective is to raise the level of the curves higher and closer to each other.

3.3.1 Design of a Laplacian Kernel to Curtail the Diffusion of Edges

A generalized parametric realization of a Laplacian kernel can be written in form of

$$L = \begin{bmatrix} \beta/2 & \alpha & \beta/2 \\ \alpha & -4(\alpha+\beta/2) & \alpha \\ \beta/2 & \alpha & \beta/2 \end{bmatrix} . \tag{3.8}$$

From this generalized Laplacian kernel, one can obtain different kernels depending on the values of the parameters α and β. For example, the Laplacian kernel L_1 can be obtained by choosing $\alpha = 1$ and $\beta = 0$. Similarly, for $\alpha = 0$ and $\beta = 1$, (3.8) yields

$$L_2 = \frac{1}{2} \begin{bmatrix} 1 & 0 & 1 \\ 0 & -4 & 0 \\ 1 & 0 & 1 \end{bmatrix} ,$$

which is also a commonly used Laplacian kernel [63]. The generalized parametric kernel given by (3.8) is a linear combination of two Laplacian kernels of L_1 and L_2 given by

$$L = \alpha L_1 + \beta L_2 . \tag{3.9}$$

In order to study the effect of this Laplacian operator (L) on the orthogonal (vertical and horizontal) and diagonal edges shown in Figure 3.1, we first obtain the response of L to each pixel numbered as 1 to 9. For this purpose we assume that structure of the edges continues beyond the 3×3 region of the image shown in this figure. The response to all the 9 pixels in the 3×3 region containing the vertical edge (Figure 3.1(b)) is given as

$$\nabla^2 I_p = \begin{cases} (\alpha+\beta)u_2 - (\alpha+\beta)u_1, & p = 1,2,3 \\ -\nabla^2 I_{p-3}, & p = 4,5,6 \\ 0, & p = 7,8,9 \end{cases} \tag{3.10}$$

and that for the pixels of the region containing the diagonal edge with $\theta = 45^\circ$ (Figure 3.1(c)) is given by

$$\nabla^2 I_p = \begin{cases} (-1)^p \left[(\beta/2)u_1 - (\beta/2)u_2\right], & p = 1, 6, 8 \\ (-1)^p[(2\alpha + \beta/2)u_2 - \\ \qquad (2\alpha + \beta/2)u_1], & p = 2, 3, 4, 5, 7 \\ 0, & p = 9\ . \end{cases} \tag{3.11}$$

Our objective is to curtail the diffusion of the edges by making $\nabla^2 u$ to be zero at all pixels on the edges and their immediate neighborhoods. This implies that we must find the values of the parameters α and β that reduces $\nabla^2 I_p$ to be zero for all values of $p \in \{1, 2, \cdots, 9\}$. It is obvious from (3.11) that for the diagonal edge with $\theta = 45^\circ$, the only values for α and β that lead to $\nabla^2 I_p = 0$ are the trivial values of $\alpha = 0$ and $\beta = 0$. The same conclusion can be reached for a diagonal edge with $\theta = -45^\circ$. Thus, for a diagonal edge, there does not exist a non-trivial Laplacian operator L that when operated on the pixels lying on the edges or those in their neighborhoods gives a zero response.

However, for a vertical edge, it is seen from (3.10) that for $\alpha = -\beta$, $\nabla^2 I_p = 0$ for all $p = 1, 2, \cdots, 9$. In this case, the Laplacian operator L as gives by (3.8) can be expressed as

$$L^{(\gamma)} = \gamma L_3\ , \tag{3.12}$$

where γ is an arbitrary constant and L_3 is a Laplacian kernel defined as

$$L_3 = \begin{bmatrix} -1 & 2 & -1 \\ 2 & -4 & 2 \\ -1 & 2 & -1 \end{bmatrix}.$$

Note that the Laplacian kernel of L_3 has been used in the literature [92] for estimating of the noise variance of images. It is now clear from the above study as to why L_3 provides a better estimate the noise variance in images. As a matter of

fact, it eliminates the effect of orthogonal edges in the Laplacian map of the images. However, our objective here is to study the effect of $L^{(\gamma)}$ in the nonlinear diffusion filter given by (3.3).

The nonlinear filter described by (3.3) has two diffusion terms, namely $(\tau c(.)\nabla^2 u)$ and $(\tau \nabla_d c(.)\nabla_d u)$, which are linearly scaled by the step-size τ. Although in practice both these terms are linearly scaled by the same step-size τ, the possibility of scaling each term by a different scale factor has been pointed out in [85] in order to provide some controlling mechanism to the forward and backward diffusion components of the filtering process. In (3.3), when $L^{(\gamma)} = \gamma L_3$ is used, the first diffusion term becomes $(\tau' c(.)(L_3 * u))$, where $\tau' = \tau\gamma$ and $*$ represents the convolution operation. Thus, the approximation of the Laplacian operator by $L^{(\gamma)}$ effectively provides two different scaling factors, τ' and τ, to the two diffusion terms, respectively and Laplacian operator replaced by operator L_3. Now we consider again orthogonal and diagonal edges of images as shown in Figure 3.2 to examine the effect of $L^{(\gamma)}$ on nonlinear diffusion of images in the presence of edges. For this purpose, we chose $\gamma = 1$.

The image of Figure 3.2(a) is filtered using (3.3) with the step-size $\tau = 0.1$ which employs the diffusivity function of (3.7) with $K = 10$. Figures 3.3(a) and 3.3(b) show the filtered images after 25 and 100 iterations, respectively, resulting from the use of the Laplacian operators L_3. As expected, L_3 is capable to preserve the vertical edge of the image, since $\nabla_d c(.)$ and $u * L_3$ are exactly zero meaning that the diffusion process is completely halted at the edge. The same result could be observed in the presence of a horizontal edge in the image.

Next, the filter given by (3.3) with the same parameter settings as used for the orthogonal edge is applied to the image of Figure 3.2(b) i.e. an image with a diagonal edge ($\theta = 45°$). The results after 25 and 100 iterations are shown in Figures 3.3(c) and 3.3(d), respectively. Even though $L^{(\gamma)}$ has been designed to preserve orthogonal edges, it is seen from these figures that the use of the Laplacian kernel does not

smooth the diagonal edge. On the contrary, it gets enhanced as a result of an inverse diffusion process taking place . However, as the number of iterations is increased, ringing artifacts are formed resulting from the up lifting and down lifting of the pixel intensities on both sides of the edge. It also seen that the phenomenon of these lifting of the pixel intensities violates the extremum principle [93, 94]:

$$min(u^{(0)}) \leq u^{n}_{(i,j)} \leq max(u^{(0)}) \ \ \forall n \in [0, +\infty] \ . \tag{3.13}$$

It is known that the nonlinear diffusion filter (3.3) using the diffusivity function of (3.7) and the Laplacian kernel L_1 supports the extremum principle [64] even though it performs inverse diffusion on regions where $\|\nabla u\| > K$. In the next subsection, we will determine the condition under which the nonlinear diffusion filter does not violate the extremum principle so that a scheme overcoming this problem could be devised.

3.3.2 Analysis

We analyze the problem of the nonlinear diffusion filter violating the extremum principle when it uses $L^{(\gamma)}$ as the Laplacian kernel. For this analysis we utilize an expression of the nonlinear diffusion filter in the form of a system of ordinary differential equations given by [64]

$$\begin{aligned} \partial \mathbf{u}/\partial t &= A(\mathbf{u})\mathbf{u}, \\ \mathbf{u}(t=0) &= \mathbf{f} \end{aligned} \tag{3.14}$$

in which $\mathbf{u} = (u_1, \cdots, u_q, \cdots, u_N)$ is a vector consisting of the pixel values of the image taken column-wise such that u_q represents the pixel value at position (i, j), N denotes the total number of pixels in the image, and A is an $N \times N$ matrix with elements $a_{k,l}(\mathbf{u})$. When (3.14) employs the Laplacian kernel $L^{(\gamma)}$, the element of A

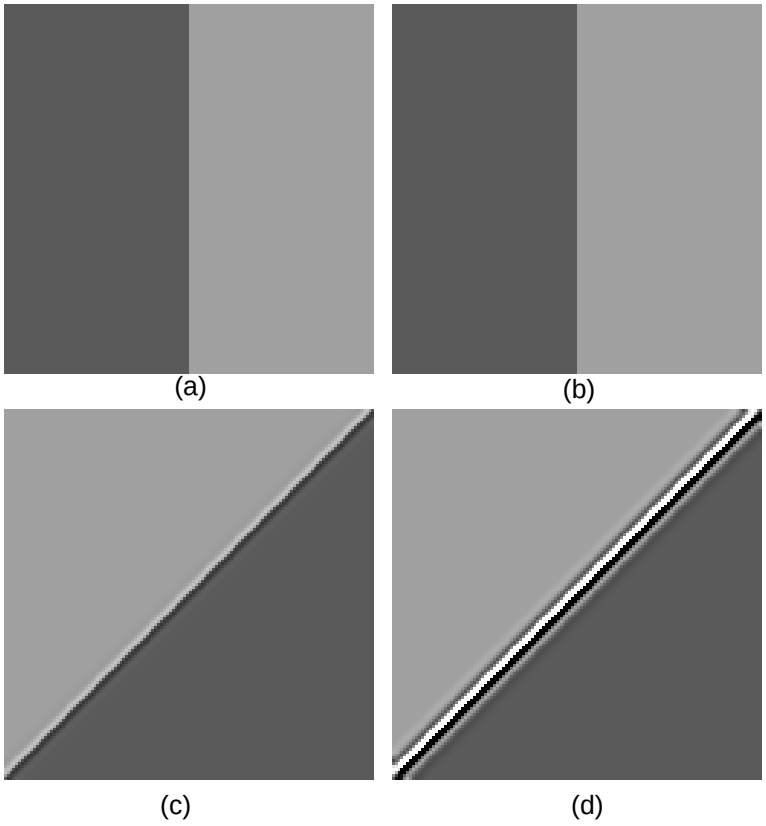

Figure 3.3: Diffusion of the image containing vertical and diagonal step edges by (3.3) using the Laplacian kernel $L^{(\gamma)}$, (a) and (c) diffused images after 25 number of iterations, (b) and (d) diffused images after 100 number of iterations.

can be expressed as

$$a_{k,l} = \begin{cases} (c_k + c_l)/2 + (2\gamma - 1)c_k, & l \in N_o(k) \\ -\gamma c_k, & l \in N_d(k) \\ -\sum_{l \in N_d(k)} \{(c_k + c_l)/2 + & \\ (2\gamma - 1)c_k\} + \sum_{l \in N_e(k)} \gamma c_k, & l = k \\ 0, & else\ , \end{cases} \tag{3.15}$$

where $N_o(k)$ and $N_d(k)$ denote the sets of the indices of the immediate neighbors of u_k in the 2-D image in the orthogonal and diagonal directions, respectively, and c_q is the diffusion coefficient at pixel position q.

In [95], it is shown that if matrix A satisfies the following conditions:

(S1) $\sum_{l=1}^{N} a_{k,l} = 0$

(S2) *$a_{k,l} \geq 0$ for all $l = 1, \cdots, N$ $(l \neq k)$ for all $k = 1, \cdots, N$ for which u_k is an extremum*

then the diffusion filter (3.14) satisfies the extremum principle. It is seen from (3.15) that the filter employing The Laplacian Kernel $L^{(\gamma)}$ always satisfies the condition (S1); however, the condition (S2) is not satisfied because of the the presence of the negative entries in A for indices $l \in N_d(k)$ and possible negative terms in A for indices $l \in N_o(k)$ whenever $\gamma < 1/4$.

In order for the filter given by (3.14) to satisfy the extremum principle, we now propose to modify the matrix A by using a function $f(u_k)$ as follows.

$$a_{k,l} = \begin{cases} (c_k + c_l)/2 + (2\gamma - 1)c_k, & l \in N_o(k) \\ -\gamma f(u_k) c_k, & l \in N_d(k) \\ -\sum_{l \in N_d(k)} \{(c_k + c_l)/2 + & \\ (2\gamma - 1)c_k\} + \sum_{l \in N_e(k)} \gamma f(u_k) c_k, & l = k \\ 0, & else \end{cases} \tag{3.16}$$

It is seen from the above equation that with the proposed modification of A, the condition (S1) is still readily satisfied. However, in order to satisfy the condition (S2), $f(u_k)$ should be capable of making the entries of A for $l \in N_d(k)$ to vanish whenever u_k is an extremum. In the next subsection, we explain how this can be accomplished by designing a data-dependent kernel and discuss its implication on the performance of the filter.

3.3.3 An Edge Adaptive Laplacian Kernel

Using the kernel $L^{(\gamma)} = \gamma(2L_1 - 2L_2)$ in (3.3), which is the fully discrete version of (3.14), we obtain

$$(u_{i,j}^{(n+1)} - u_{i,j}^{(n)})/\tau = 2\gamma\,[c(.)_{i,j}(u * L_1)_{i,j}]^{(n)} - 2\gamma\,[c(.)_{i,j}(u * L_2)_{i,j}]^{(n)} + \frac{1}{2}\left[\sum_d \nabla_d c(.)_{i,j} \nabla_d u_{i,j}\right]^{(n)} . \quad (3.17)$$

The backward Laplacian diffusion term $2\gamma\,[c(.)_{i,j}(u * L_2)_{i,j}]$ in (3.17) results from the entries corresponding to the $l \in N_d k$ (i.e. $-\gamma c_k$) and $\sum_{l \in N_e(k)} \gamma c_k$ part of the entries corresponding to $l = k$ of A. It is only these entries of A, given by (3.15) that are affected when A is modified as in (3.16) using the function $f(.)$. Thus, the proposed modification of A results in modifying (3.17) as

$$(u_{i,j}^{(n+1)} - u_{i,j}^{(n)})/\tau = 2\gamma\,[c(.)_{i,j}(u * L_1)_{i,j}]^{(n)} - 2\gamma\,[f(.)c(.)_{i,j}(u * L_2)_{i,j}]^{(n)} + \frac{1}{2}\left[\sum_d \nabla_d c(.)_{i,j} \nabla_d u_{i,j}\right]^{(n)} . \quad (3.18)$$

In essence, the proposed modification of A simply affects the backward Laplacian diffusion term by multiplying it with $f(.)$. Our objective is to make (3.18) independent of the backward Laplacian diffusion term at an extremum of u by letting $f(.)$ assume a value of zero at such pixel positions of the image.

In [95], a non-standard approximation of the gradient modulus is suggested as

$$\widetilde{\nabla} u_{i,j} = [max(-\nabla_N u_{i,j}.\nabla_S u_{i,j}, 0) + max(-\nabla_E u_{i,j}.\nabla_W u_{i,j}, 0)]^{1/2} , \quad (3.19)$$

which assumes the value of zero at extremum of u. Using this approximation for the gradient, $\widetilde{\nabla} u_{i,j}$, we propose a function $f(.)$ to have the following form:

$$f(u_{i,j}) = c(0) - c(\widetilde{\nabla} u_{i,j}) . \quad (3.20)$$

Thus, with this choice of $f(u_{i,j})$, the backward Laplacian diffusion term of the filter (3.18) is eliminated at extermum of u and the filter satisfies the extremum principle. In the following, we investigate the behavior of this modified filter given by (3.18).

Let us consider the value $u_{r,s}$ that is an edge pixel. Then, it is easy to see that the approximate gradient modulus given by (3.19) for such a pixel is zero; thus, the function $f(u_{r,s})$ given by (3.20) assumes a zero value. Since, as discussed in Section II, the third diffusion term in (3.18) vanishes for an edge pixel, (3.18) assumes the following form

$$(u_{r,s}^{(1)} - u_{r,s}^{(0)})/\tau = 2\gamma \left[c(.)_{r,s}(u * L_1)_{r,s}\right]^{(0)} \ , \tag{3.21}$$

for the first iteration of the filtering operation that is, it has the forward diffusion. Thus, unlike the filtering operation performed by (3.17) in which the diffusion process on the orthogonal edges is completely halted, in the filtering operation performed by the filter (3.18) all the edge pixels including the orthogonal edge pixels would undergo the diffusion operation. However, in order to make the filter (3.18) not to perform more diffusion on the edges than done by (3.4), one has to chose the value of $\gamma \leq 1/2$. But, a small value of γ, on the other hand, would impact negatively on the noise filtering capability of (3.18) for the smooth regions of the image.

In order to increase the noise reduction performance of (3.18) without hindering its edge preservation capability, it is required to devise a mechanism of increasing the value of γ beyond 0.5 without increasing the forward diffusion on the edges. For $\gamma > 1/2$, the forward Laplacian diffusion performed by (3.18) is bigger than that performed by the nonlinear diffusion filter (3.4). In order to eliminate the impact of the extra diffusion on the edges, we modify the forward diffusion term $2\gamma c(.)_{i,j}(u*L_1)_{i,j}$ of (3.18) as

$$c(.)_{i,j}(u * L_1)_{i,j} + f(.)(2\gamma - 1)c(.)_{i,j}(u * L_1)_{i,j} \ , \tag{3.22}$$

where the first term is exactly same as the forward Laplacian diffusion term of (3.3) and the second term is the extra diffusion part in (3.18). Thus, with the modified

forward Laplacian diffusion term, its negative effect on the edges would not exceed that of (3.3) because of the presence of $f(.)$, whereas the performance of (3.18) in smooth regions should improve because of the value of $\gamma > 1/2$. The nonlinear diffusion filter (3.18), after this modification, becomes

$$(u_{i,j}^{(n+1)} - u_{i,j}^{(n)})/\tau = [c(.)_{i,j}(u * L_1)_{i,j}]^{(n)} + \{f(.)\,[(2\gamma - 1)c(.)_{i,j}(u * L_1)_{i,j} - 2\gamma c(.)_{i,j}(u * L_2)_{i,j}]\}^{(n)} + \frac{1}{2}\left[\sum_d \nabla_d c(.)_{i,j} \nabla_d u_{i,j}\right]^{(n)} . \quad (3.23)$$

It is important to note that the filter (3.23) still satisfies the extremum principle, since the backward Laplacian diffusion term is still intact compared to that in filter (3.18). The purpose of modifying (3.18) into (3.23) has been to improve the noise reduction capability of the resulting filter by using a larger value of the parameter γ. We would now examine as to how this modification affects the performance of (3.23) in terms of processing orthogonal edges. Since, $L_3 = 2L_1 - 2L_2$, the second term on the right side of (3.23) can be simplified as

$$f(.)\,[(2\gamma - 1)c(.)_{i,j}(u * L_1)_{i,j} - 2\gamma c(.)_{i,j}(u * L_2)_{i,j}] = f(.)\,[c(.)_{i,j}\gamma(u * L_3)_{i,j} - c(.)_{i,j}(u * L_1)_{i,j}] \ , \quad (3.24)$$

As at the orthogonal edges $(u * L_3) = 0$, the diffusion performed on these edges by (3.23) is independent of the value of γ, and considering the fact that for many diffusion functions $c(.)$ assume a value in $(0, 1]$ with $c(0) = 1$, i.e., $f(.) = 1 - c(\widetilde{\nabla} u)$, the Laplacian diffusion process carried out by filter (3.23) on an orthogonal edge is given by

$$[c(.)_{i,j}(u * L_1)_{i,j}] - f(.)\,[c(.)_{i,j}(u * L_1)_{i,j}] = c(\|\nabla u_{i,j}\|)_{i,j} c(\widetilde{\nabla} u_{i,j})_{i,j}(u * L_1)_{i,j} \, . \quad (3.25)$$

If we compare the diffusion coefficient $c(\|\nabla u_{i,j}\|)c(\widetilde{\nabla} u_{i,j})$ of (3.23) with the diffusion coefficient $c(\|\nabla u_{i,j}\|)$ in (3.4), the diffusion performed on the orthogonal edges by (3.23) is less than that performed by (3.4) from iteration 2 onward, since $c(\|\nabla u_{i,j}\|)^{(n)} > c(\|\nabla u_{i,j}\|)^{(n)} c(\widetilde{\nabla} u_{i,j})^{(n)}$.

Before closing this section, we make an explicit comparison of the filters given by (3.3) and (3.23). By combining the first two terms on the right side of (3.23), we have a single Laplacian diffusion term in the form of $c(.)(u * L)_{i,j}$, where $L_{i,j}$ is given by

$$L_{i,j} = L_1 - f(u_{i,j})((2\gamma - 1)L_1 - 2\gamma L_2) \ . \tag{3.26}$$

Recall that in (3.3), the Laplacian operation is performed by using the kernel L_1 as $\nabla^2 u = L_1 * u_{i,j}$. Note that if kernel L_1 in (3.3) is replaced by $L_{i,j}$, then (3.3) becomes the filter given by (3.23). In a view of the fact that $L_{i,j}$ depends on $u_{i,j}$, hereafter we refer to it as the edge adaptive kernel.

3.4 Simulation Results

In this section, we study the effect of the proposed edge-adaptive kernel on the filtering performance of three nonlinear diffusion filters. The nonlinear diffusion filters considered for this purpose are the classical filter proposed by Perona and Malik [35], the anisotropic filter introduced by Carmona and Zhong [83] and a filter due to Hongchuan and Chua [85]. The performance of these filters are examined when the kernel L_1 of these filters is replaced by the proposed one. Their performances are measured in terms of the SNR representing the noise removal capability of the filters, and a figure of merit (FOM) index introduced by Pratt's [11] that represents the edge preservation capability of the filters. The SNR is defined as

$$SNR = 10log_{10}\left(var(\widehat{u})/var(I - \widehat{u})\right) \ , \tag{3.27}$$

where $\widehat{u}$ and I denote, respectively, the denoised and noiseless images, $var(.)$ and $avg(.)$ denote, respectively, the variance and average of the pixel values of the associated image. The index FOM is defined in [11] as

$$FOM = \frac{1}{max(u_D, u_I)} \sum_{i=1}^{u_D} \frac{1}{1 + \phi d_i^2} , \tag{3.28}$$

where u_D is the number of detected edge points, u_I the number of edge points in the image I, ϕ is a positive scaling factor often chosen to be 1/9, and d_i the distance between the i^{th} detected edge pixel in $\widehat{u}$ and the corresponding pixel in I. For the evaluation of FOM, the *Sobel* operator is used for the edge detection. Filters in these experiment are implemented using a MATLAB 2008Ra simulation platform on a Windows-based 64-bit icore5 machine with 4-GB RAM.

3.4.1 The Nonlinear Diffusion Filter of Perona and Malik [35]

The proposed edge adaptive kernel used in the filter given by (3.23) has a parameter γ. Recall that the lower limit of 1/4 of this parameter is dictated by the extremum principle. On the other hand, a larger value of this parameter within a limit ensuring the numerical stability of the discrete model of the filter improves the noise reduction capability of the filter. In order to see the impact of the value of γ chosen on the diffusion of orthogonal and diagonal edges, we again consider the synthetic images shown in Figures 3.2(a) and 3.2(b) containing vertical and diagonal edges, respectively. These images are diffused by employing the filters given by (3.23) and (3.3) using the diffusivity function given by (3.7) for the value of contrast parameter K chosen in the interval $[5, 25]$ and for values of γ in the range $[0.5, 1.5]$. The filtering is performed for $n = 30$ iterations and the time step size $\tau = 0.1$.

The variance of the diffused images as a function of K for different values of γ is depicted in Figure 3.4 for the vertical and diagonal edges. It is seen from this figure that the variance of the images diffused by the proposed filter for both the diagonal

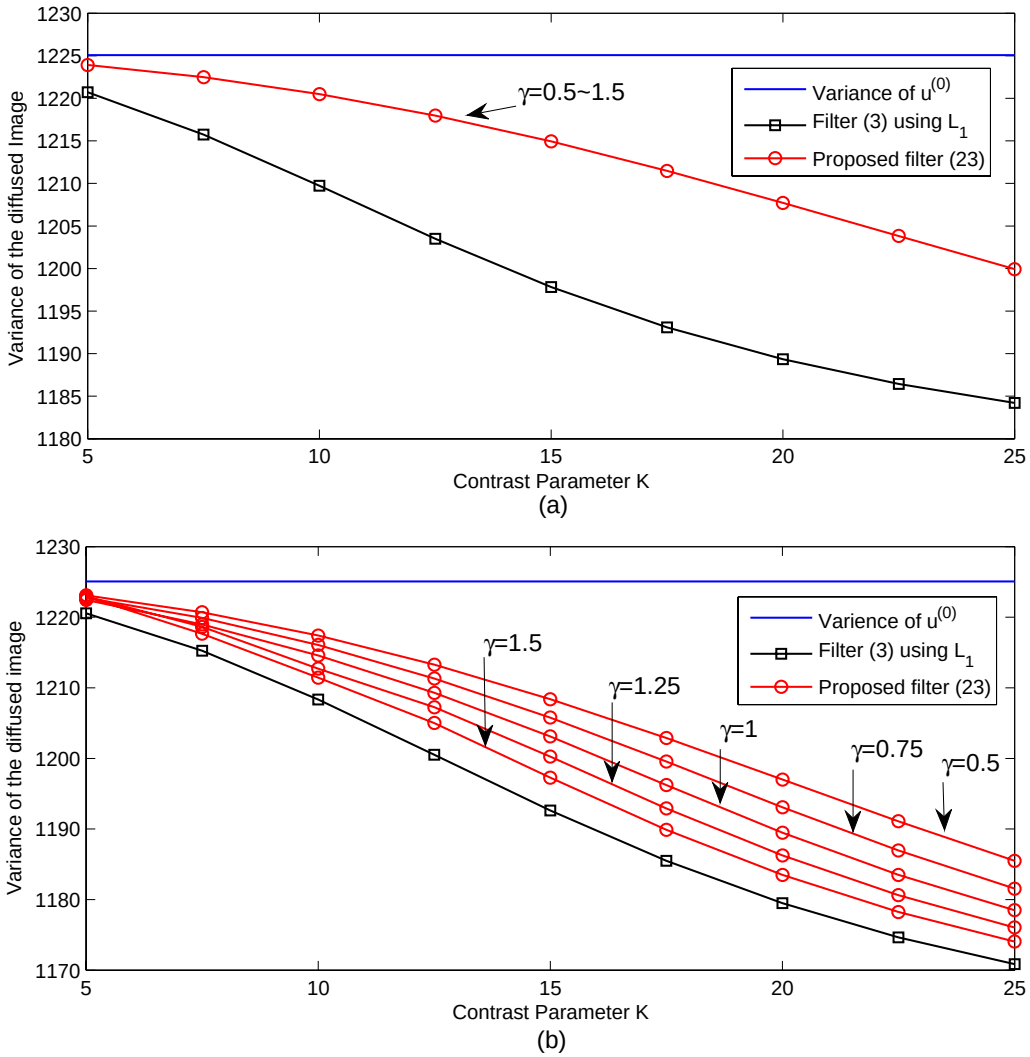

Figure 3.4: The variance of the image as a function of the contrast parameter K and γ illustrating the effects of using the L_1 and $L_{i,j}$ kernels on the diffusion precess of (3.3) for an image having (a) vertical edge and (b) a diagonal edge.

and vertical edges is consistently higher than that obtained by using (3.3) indicating a smaller diffusion of the edges by the proposed filter. Also, as expected, the diffusion performed by (3.23) on the vertical edge is independent of the choice of the value γ (Figure 3.4(a)). Even though the noise reduction capability of the proposed filter is, in general, enhanced at the expense of a reduced edge preservation capability by choosing a larger value of γ, it is seen from Figure 3.4(b) that even for $\gamma = 1.5$, the diffusion of the diagonal edge by the proposed filter is smaller than that by (3.3).

Therefore, the value of γ for all of the simulation study of this section is chosen to be 1.5.

In order to examine the performance of the filters given by (3.3) and (3.23), we use the regularized version [73], $c(\|\nabla(G_\sigma * u)\|)$, of the diffusivity function given by (3.7) in which G_σ denotes the Gaussian kernel with standard deviation σ. The value of σ is chosen to be 1. The value of the contrast parameter K is set using the so-called threshold freezing scheme given in [96]:

$$K^{(n)} = \frac{1}{\epsilon + \chi \cdot n \cdot \tau} \,, \tag{3.29}$$

where $\epsilon = 10^{-10}$ and χ is a threshold parameter, which provides a non trivial steady state solution of the nonlinear diffusion filter in a finite number of iterations. The iterative filtering process is stopped once the condition $||u^{(n)} - u^{(n-1)}||/||u^{(n-1)}|| \leq 10^{-4}$ is satisfied. The time step size τ is chosen to be 0.05.

In this simulation study, the synthetic images of *disk*, and *Flingstone*, a natural image *House*, and an organic super-conductor (OSC) image given in [97] are chosen. Table 3.1 gives a comparative performance of the two schemes, when L_1 and the proposed kernel are used, to filter these images corrupted by white Gaussian noise (AWGN) with standard deviation $SD = 15$ and 25. For the purpose of comparison, the SNR and the corresponding FOM values of the filtered images are obtained at the threshold values $\chi = \chi_{opt}$ that provide the largest possible SNR for the filtered images. This table also depicts the total number of iteration meeting the stopping condition specified above and CPU time. It is seen from this table that the proposed filter yields the SNR and corresponding FOM values that are consistently higher than that provided by the filter using kernel L_1. On the average, SNR and FOM values obtained by the filter using the proposed kernel are, respectively, 0.98dB and 6.98% higher than when the L_1 kernel is used. However, it is noted that this improvement in the performance of the filter is achived at the expense of an increased computantinal complexity. The proposed scheme results have a higher number of iterations and a

CPU time that is on the average 46% larger.

Table 3.1: Quantitative comparison of the results obtained by using the Laplacian kernel L_1 and the proposed kernel $L_{i,j}$ in filter (3.3)

Noise level	Degraded Image				Filtered Image			
	Image	SNR(dB)	Kernel	χ_{opt}	SNR(dB)	FOM	n	Time(s)
SD = 15	*House*	10.17	L_1	0.40	17.60	0.7133	62	1.12
			Proposed	0.23	17.96	0.7688	75	1.71
	OSC	11.47	L_1	0.56	17.08	0.7495	67	3.20
			Proposed	0.52	17.34	0.7817	70	4.13
	Disk	15.95	L_1	0.28	28.43	0.8491	78	1.35
			Proposed	0.05	31.16	0.8579	90	2.02
	Flintstone	14.13	L_1	0.55	17.97	0.8183	51	7.22
			Proposed	0.45	18.09	0.8624	56	9.11
SD = 25	*House*	6.41	L_1	0.2	15.46	0.6184	89	1.60
			Proposed	0.08	16.11	0.7005	117	2.81
	OSC	7.52	L_1	0.28	14.33	0.6190	60	4.56
			Proposed	0.22	14.52	0.6976	68	6.48
	Disk	11.71	L_1	0.17	25.23	0.8161	108	1.9
			Proposed	0.025	28.56	0.8177	119	3.1
	Flintstone	9.97	L_1	0.3	15.48	0.7035	69	9.71
			Proposed	0.21	15.65	0.7831	82	13.29

Figure 3.5 depicts the perceptual quality of the image *house* processed by the two filters. The original image and the one degraded by a noise with $SD = 25$ are shown in Figures 3.5(a) and (b), respectively. Figures 3.5(c) and (d) show the images processed by filters (3.3) and (3.23), respectively, that employ the optimal values of χ of the respective filters, that is, 0.2 and 0.08, respectively. It is seen from these two images that filter (3.3) is not as effective in removing the noise and preserving the edges as filter (3.23). By increasing the value of χ to a value higher than χ_{opt}, the noise reduction ability of the filters would naturally be reduced. However, the resulting reduction of the diffusion on the edges should increase the FOM value compared to that of χ_{opt}. To see the effect of increasing χ above χ_{opt}, we increase the value of χ in filter (3.3) from its optimal value of 0.2 to 0.35 at which the FOM value of the processed image by this filter becomes almost equal to the FOM value of the filter (3.23) at its optimal value i.e. 0.7005. It is seen from the the resulting processed image, shown in Figure 3.5(e), that the noise reduction ability of the filter (3.3) is

considerably reduced, and quantitatively the SNR value gets reduced from its optimal value of $15.46dB$ (Figure 3.5(c)) to $14.75dB$. Figure 3.5(f) shows the processed image by the filter (3.23) with the value of χ increased from its optimal value for filter (3.23) to that of for filter (3.3) i.e. $\chi = 0.2$. It is seen from this figure that as expected more noise is left behind compared to that in Figure 3.5(d) as a result of the reduction of the diffusion, which is particularly visible of the edges. However, the FOM value of the image in Figure 3.5(f) is 0.7606, which is larger than the value of 0.7006 for the image in Figure 3.5(e).

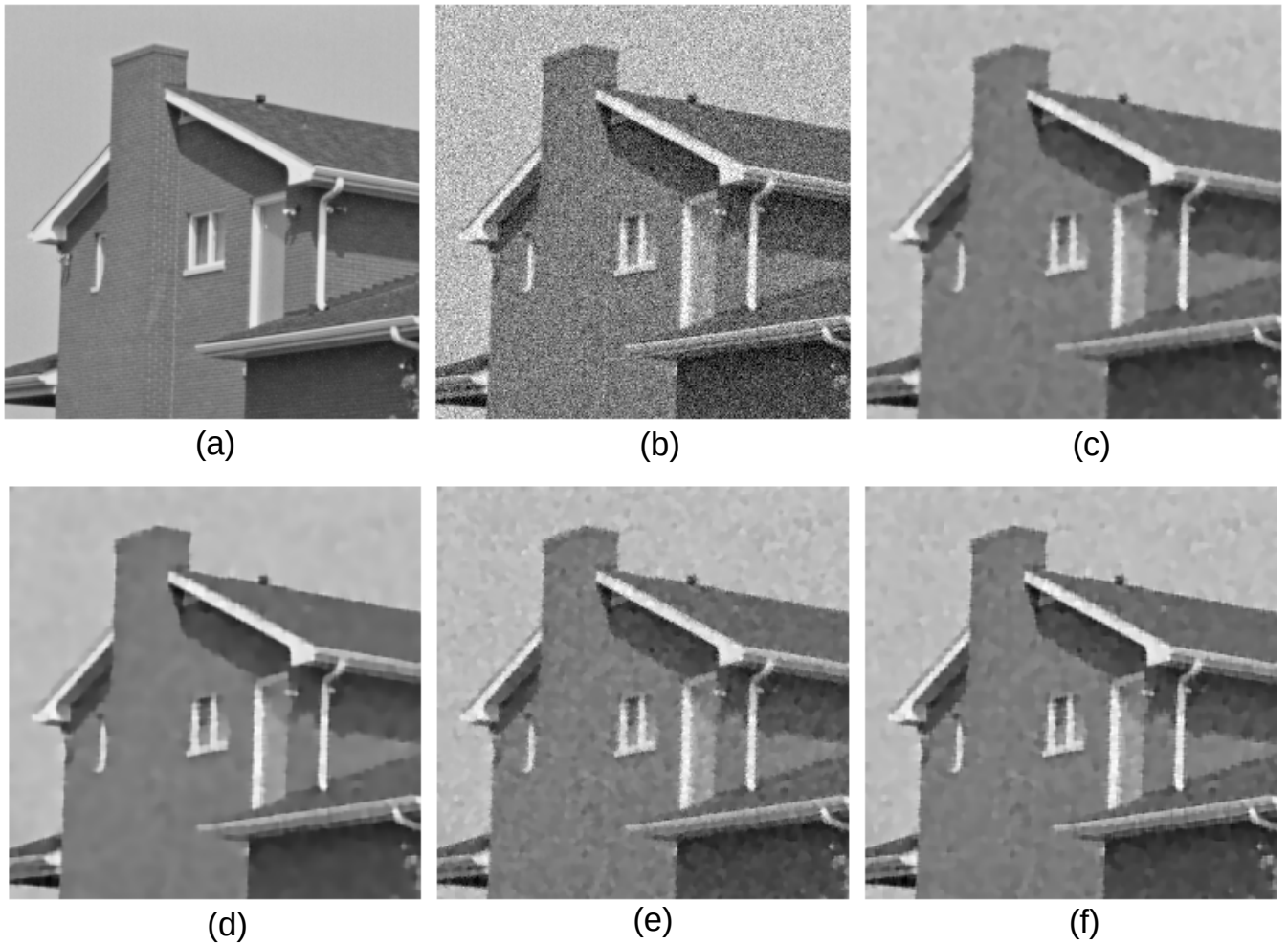

Figure 3.5: The perceptual quality of the processed image *House*. (a) Original image. (b) Image contaminated by AWGN with SD=25. (c) Image denoised using (3.3) with $\chi_{opt} = 0.2$. (d) Image denoised using (3.23) with $\chi_{opt} = 0.08$. (e) Image denoised using (3.3) with $\chi = 0.35$; (f) Image denoised using (3.23) with $\chi = 0.2$.

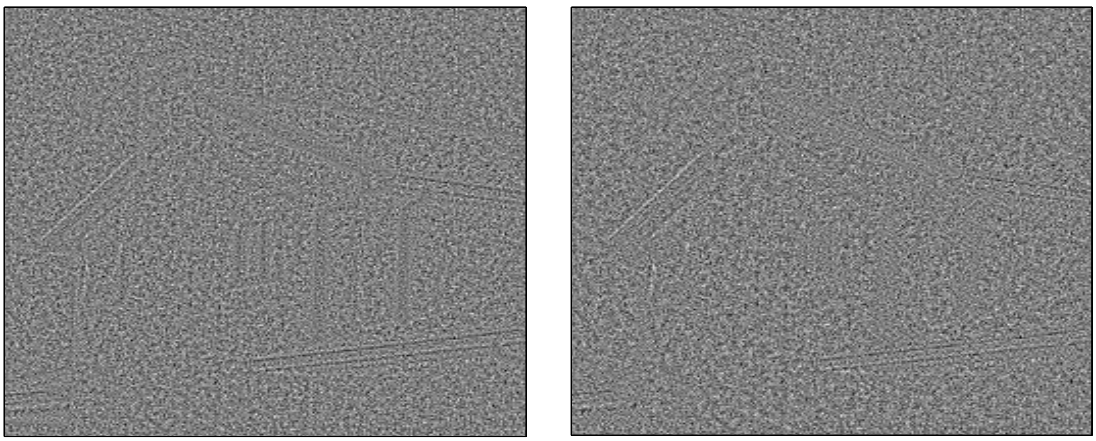

Figure 3.6: The quality of edge preservation illustrated by the residual image $\widehat{u} - u^{(0)}$. The residual of the image processed by (a) filter (3.3) and (b) filter (3.23).

In order to further compare the edge preservation capability of the two filters, the residual images $\widehat{u} - u^{(0)}$ corresponding to images processed by filters (3.3) and (3.23) at χ_{opt} are obtained and shown in Figure 3.6. It is clear from this figure that the diffusion process of the image edges as carried out by (3.3) is stronger than that by (3.23).In order to quantitatively analyze the results of the filtering operations carried out by (3.3) and (3.23), the variance of the residual image, $var(\widehat{u} - u^{(0)})$, and absolute value of their correlation with the estimated image, $|corr(\widehat{u} - u^{(0)}, \widehat{u})|$, are obtained. These values are 591 and 0.05, respectively, resulting from the filtering operation carried out by (3.3) and 616 and 0.01, respectively, resulting from the filtering operation of (3.23). A higher value of the variance along with simultaneously lower value of the correlation in the case when the filtering is carried out by (3.23) indicates the effectiveness of the new kernel in both edge preservation and noise reduction.

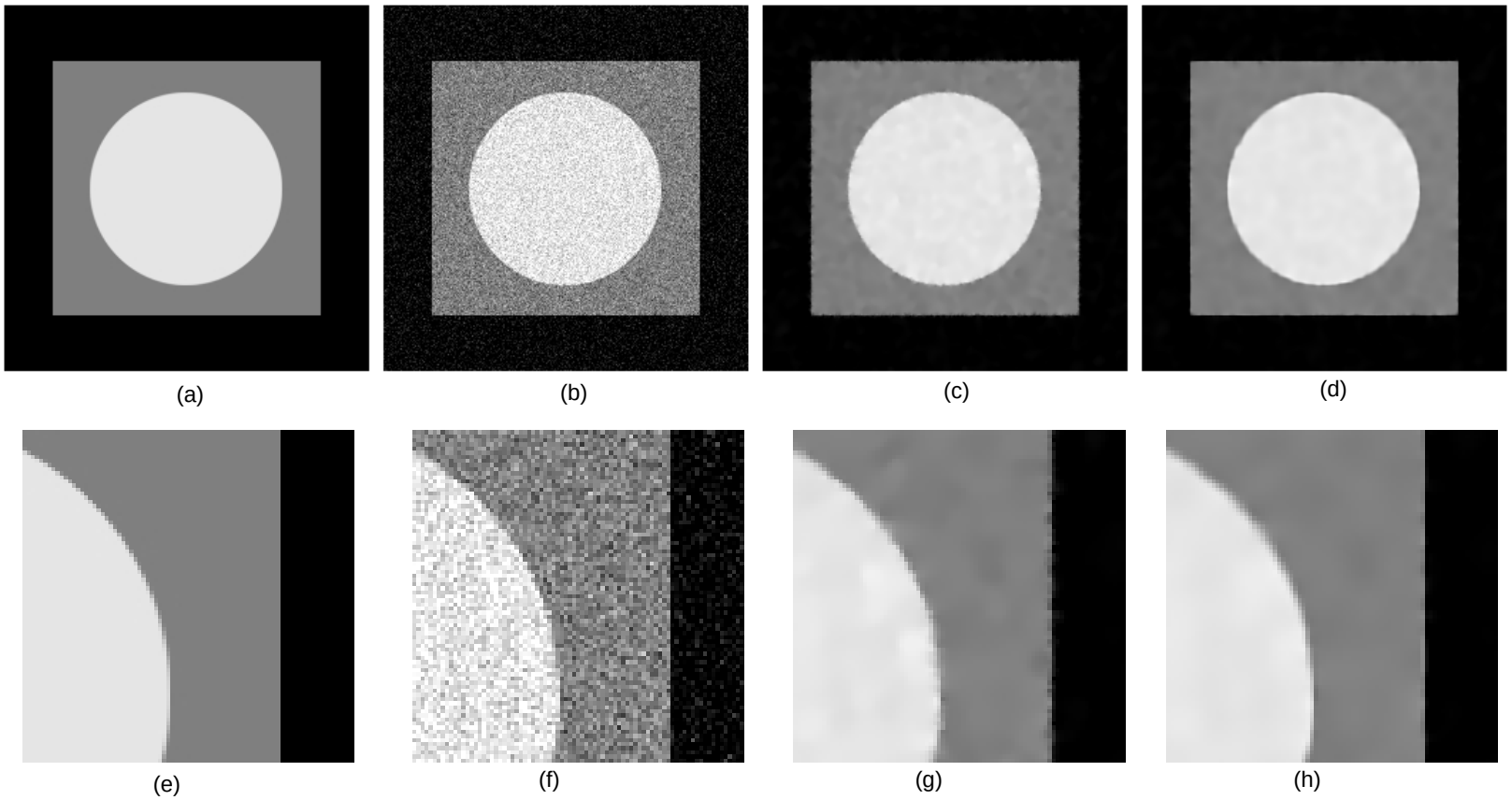

Figure 3.7: The perceptual quality of the processed image *Disk*.(a) Original image. (b) Image contaminated by AWGN with $SD = 25$. (c) Image denoised by (3.3). (d) Image denoised by (3.23). Images in (e), (f), (g), and (h) are the magnified version of a part of the images in (a), (b), (c), and (d), respectively.

For images containing only high contrast edges such as image *Disk*, the diffusion coefficients corresponding to the edge pixels is sufficiently small and as a result the edge preservation of the filter by using Laplacian kernel L_1 would not be substantially different from that using the proposed kernel as quantitatively evaluated by FOM value in Table 3.1. However, in this case the advantage of using the proposed kernel instead of kernel L_1 is on the better noise reduction ability of the filter, which can make a considerable difference in SNR value of the images. In Figure 3.7, the results of these filters for noise level $SD = 25$ are shown. It is seen from these results that even though both filters are capable of preserving edges during the diffusion process, a significant amount of the noise still remains on the edge pixels of the diffused image obtained by (3.3), which is perceptually more visible as seen from the magnified region of the images shown in Figure 3.7(g). On the other hand, the proposed filter effectively removes the noise and preserves the edges (Figure 3.7(h)).

3.4.2 The Anisotropic Filter of Carmona and Zhong [83]

As mentioned earlier, the proposed edge-adaptive kernel $L_{i,j}$ can also be used in nonlinear diffusion settings other than the one given in (3.3). In the following, we show how the proposed kernel can be used in the anisotropic filter of Carmona and Zhong [83]. The PDE of this filter is given by

$$u_t = a\left(\|\nabla u\|\right)\left(b\left(\|\nabla u\|\right)u_{\xi\xi} + c\left(\|\nabla u\|\right)u_{\eta\eta}\right)\ , \tag{3.30}$$

where $a(.)$, $b(.)$ and $c(.)$ are the diffusivity functions that provide a great deal of flexibility in controlling the diffusion process of the images. These diffusivity functions can be chosen in a way such that the image edges are significantly diffused in the direction of their level sets than in the direction of their gradient. Introducing the notation $\nabla^2 u$ in (3.30) using the fact that $\nabla^2 u = u_{\xi\xi} + u_{\eta\eta}$, we have

$$u_t = a\left(\|\nabla u\|\right)\left(c\left(\|\nabla u\|\right)\nabla^2 u + \left(b\left(\|\nabla u\|\right) - c\left(\|\nabla u\|\right)\right)u_{\xi\xi}\right)\ . \tag{3.31}$$

Now, in our simulation of the filter of Carmona and Zhong given by the above equation, we use the kernel L_1 and the proposed kernel $L_{i,j}$ to approximate the Laplacian operator. Note that the use of the approximation of the second-order derivatives in the direction of the level set and gradient given by

$$u_{\xi\xi} = \frac{u_{xx}u_y^2 - 2u_x u_y u_{xy} + u_{yy}u_x^2}{u_x^2 + u_y^2} \tag{3.32}$$

and

$$u_{\eta\eta} = \frac{u_{xx}u_x^2 + 2u_x u_y u_{xy} + u_{yy}u_y^2}{u_x^2 + u_y^2} \tag{3.33}$$

ensures that the filter given by (3.30) or (3.31) employs the L_1 kernel. In order to use the proposed kernel, we use $L_{i,j}$ in (3.31) to approximate the Laplacian operator and (3.32) for $u_{\xi\xi}$.

The parameter settings used for $L_{i,j}$ to perform the Laplacian operator ∇^2 are the same as that used in Section 3.4.1 except that the contrast parameter K is now set to unity. The diffusivity function $a(\|\nabla u\|)$ is chosen to be the same as in [83], i.e., $a(\|\nabla u\|) = \left[K^2/\left(K^2 + \|\nabla u\|^2\right)\right]^{1/2}$ with K given by (3.29), $b(\|\nabla u\|)$ is set to be unity, and $c(\|\nabla u\|)$ is given by (3.7) with K set to have a value of 10. The time step size is chosen to be 0.05 for the first 50 iterations and 0.25 afterward. The stopping criterion used in the filter simulation is the same as that in Section 3.4.1.

Table 3.2 gives the quantitative results in terms of the SNR and FOM of the four images degraded by AWGN with $SD = 25$ and then processed by the Carmona and Zhang filter employing the L_1 and $L_{i,j}$ kernels. It is seen from this table that replacing the kernel L_1 by $L_{i,j}$ enables the Carmona and Zhang filter to perform consistently better in processing all the four images. On the average, the proposed kernel yields the values of the SNR and FOM that are, respectively, 0.76 dB and 5.3% higher than when the kernel L_1 is employed. However, the convergence rate of the filter using the proposed kernel is lower than that when L_1 used, and this is reflected in making the computational time of the filter with $L_{i,j}$ kernel to be 24.5% higher.

Table 3.2: Quantitative comparison of the results obtained by using the Laplacian kernel L_1 and the proposed kernel $L_{i,j}$ in filter (3.31)

Noise level	Degraded Image				Filtered Image			
	Image	SNR(dB)	Kernel	χ_{opt}	SNR(dB)	FOM	n	Time(s)
SD = 25	*House*	6.41	L_1	0.33	15.14	0.6095	185	2.34
			Proposed	0.21	15.76	0.6682	193	3.04
	OSC	7.52	L_1	0.43	14.42	0.6198	258	10.10
			Proposed	0.31	14.74	0.6484	273	12.56
	Disk	11.71	L_1	0.2	27.04	0.8336	155	1.93
			Proposed	0.1	28.46	0.8368	156	2.43
	Flintstone	9.97	L_1	0.4	15.23	0.6843	172	18.66
			Proposed	0.3	15.73	0.7301	178	19.27

3.4.3 GVF-based Anisotropic Filter [85]

Nonlinear diffusion filters can be used for simultaneous deblurring and denoising, since they can be set to perform an inverse diffusion on the edges. One of the techniques for performing deblurring-denoising, introduced by Yu and Chua [85], is the gradient vector flow (GVF)-based anisotropic diffusion filter given by

$$u_t = c\left(\|\nabla u\|\right)\nabla^2 u - \vec{v}\cdot\nabla u\ , \tag{3.34}$$

where $\vec{v}$ is a gradient vector flow field calculated through an evolutionary process given by

$$\begin{aligned}\vec{v}_t &= \mu\nabla^2\vec{v} - \left(\vec{v} - \nabla E\right)\|\nabla E\|^2 \\ \vec{v}\ (t=0) &= \nabla E\ ,\end{aligned} \tag{3.35}$$

and E is the image edge map defined by

$$E = 1 - \frac{1}{\sqrt{2\pi}K}e^{(-\|\nabla u\|^2/2K^2)}\ . \tag{3.36}$$

In (3.35), μ is a positive blending coefficient used to smoothen the GVF field, $\vec{v}$. The deblurring process performed by (3.34) is due to the inverse diffusion of the edges carried out by the second term of right of (3.34).

The filter given by (3.34) has a Laplacian forward diffusion term, $c(.)\nabla^2 u$, which in

Table 3.3: Quantitative comparison of the results obtained by the filter (3.34) using kernels L_1 and the proposed kernel $L_{i,j}$

Degraded Image				Filtered Image		
Image	SNR(dB)	FOM	Kernel	SNR(dB)	FOM	Time(s)
House	8.85	0.5039	L_1	13.48	0.4748	2.16
			Proposed	14.13	0.5484	2.51
OSC	8.71	0.2816	L_1	10.45	0.3043	4.87
			Proposed	11.30	0.3757	5.39
Disk	14.87	0.5804	L_1	22.22	0.7975	2.11
			Proposed	22.49	0.8015	2.45
Flintstone	9.79	0.1179	L_1	8.34	0.2106	11.37
			Proposed	11.02	0.3442	12.39

a discrete setting is implemented as $c(.)_{i,j}(u * L_1)_{i,j}$. In order to use the proposed edge-adaptive kernel, we simply replace the Laplacian kernel L_1 in this forward diffusion term by the kernel $L_{i,j}$.

In this simulation study, filter (3.34) using the L_1 and $L_{i,j}$ kernels is set up as follows:

1. The evolutionary processes of (3.34) and (3.35) are discretized in the temporal domain using the forward Euler approximation with the time-step size τ set to 0.1

2. The spatial derivatives in (3.34) and (3.35) are based on the central difference operators with a reflective boundary condition.

3. The total number of iterations for the discretized diffusion precess of (3.34) is chosen to be 50 with the value of $\vec{v}$ updated after each 10 iterations using (3.35). The total number of iterations for the discretized realization of (3.35) is chosen to be 20.

4. The blending coefficient, μ, in (3.35) is set to unity.

5. The diffusivity function is computed as $c\left(\|\nabla u\|\right) = e^{(\|\nabla u\|/2K^2)}$ with the value of K at each iteration set to the 80% value of the integral of the gradient magnitude

of the image. The same value of K is also used in (3.36) for the evaluation of E.

6. Parameter settings used for the $L_{i,j}$ kernel are the same as those used in Section 3.4.2.

In order to see the effect of the proposed kernel in the deblurring-denoising process of (3.34), the same four images as considered earlier are first blurred using a 15×15 Gaussian kernel with the standard deviation of 1.5 and then contaminated with an AWGN having $SD = 15$. Table 3.3 gives the quantitative results for the four images in terms of the SNR and FOM. It is seen from this table that the use of the proposed kernel in the filtering process of (3.34) yields the values of SNR and FOM that are consistently better than that in the case when the L_1 kernel is used. On the average, the SNR and FOM values are, respectively, 1.1 dB and 25.73% higher. This improvement in the performance of the filter using the proposed kernel is achieved at the expense of a modest increase of only 10% in the comutational time. Figure 3.8 depicts the perceptual quality of the image *OSC* processed by (3.34) using the L_1 and $L_{i,j}$ kernels. The original test image is shown in Figure 3.8(a) and the corresponding degraded image (blurred and noise contaminated) is shown in Figure 3.8(b). Figures 3.8(c) and (d) show the images resulting from the processing of image of Figure 3.8(b) by the filter (3.34) with the L_1 and $L_{i,j}$ kernels, respectively. It is seen from these two processed images that the proposed kernel is more effective in deblurring the edges.

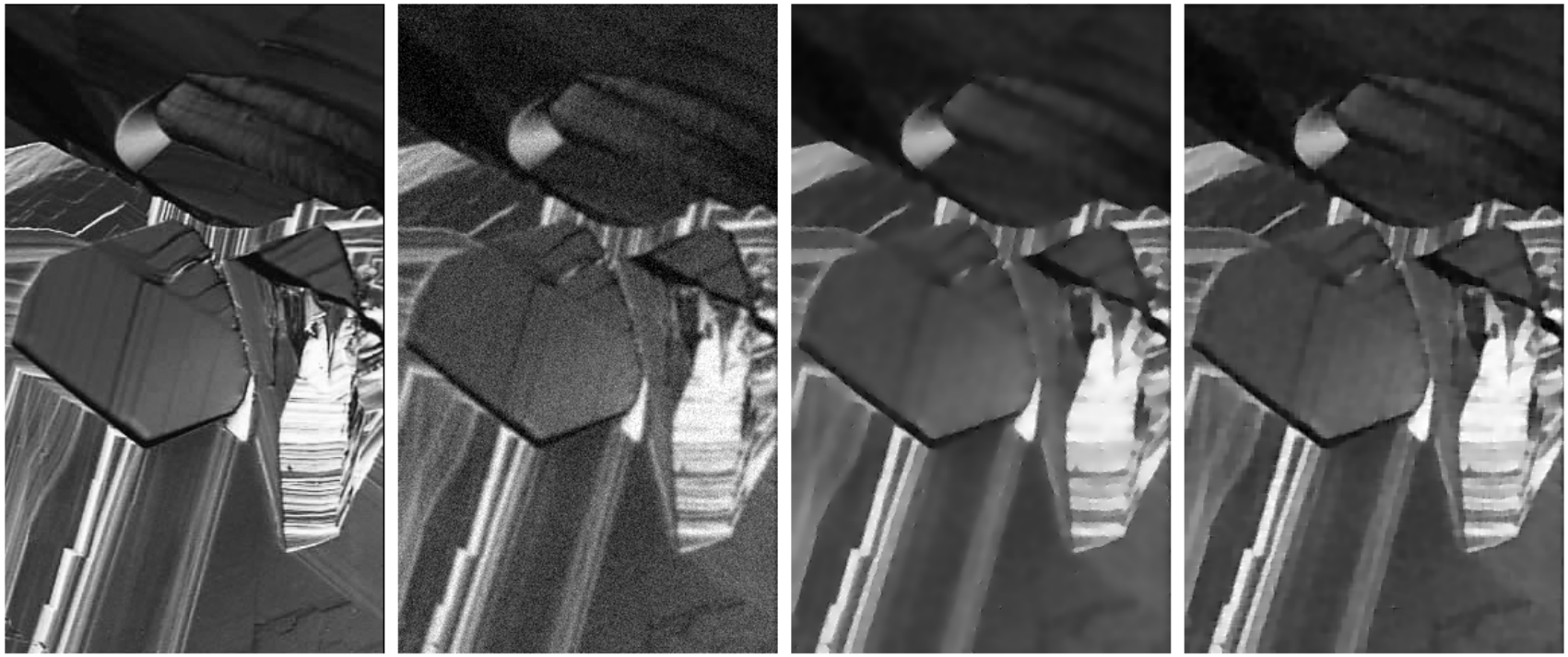

Figure 3.8: The perceptual quality of an image restored by (3.34) using the L_1 and $L_{i,j}$ kernels. (a) The original image OSC. (b) Degraded image blurred by the 15×15 Gaussian kernel with $SD = 1.5$ and contaminated by AWGN with SD=15. (c) Image processed by (3.34) using L_1. (d) Image processed by (3.34) using $L_{i,j}$.

3.5 Summary

In this chapter, a new scheme to enhance the edge-preservation capability of nonlinear diffusion filters has been developed. In contrast with the existing methods for increasing the edge preservation capability of nonlinear diffusion filters in which the focus is on significantly reducing the value of diffusion coefficient at the edges, the new scheme is motivated by the result of a study on the impact of the anisotropic behavior inherent in the discrete approximations of the Laplacian operator on the diffusion of the edges. The study has shown that the Laplacian kernel when it operates on pixels of the orthogonal edges results in a smaller diffusion of these pixels compared with the case of diagonal edges. Motivated by this result, a new Laplacian kernel has been designed, which when operated on pixels of the orthogonal edges yields a zero response. It has been shown that, although the filter employing this kernel completely halts the diffusion process of the orthogonal edges, the filter itself in this case does not satisfy the extremum principle. This problem has been analytically investigated to drive a sufficient condition for the observance of the extremum principle, and eventually, to propose an edge-adaptive Laplacian kernel. To demonstrate the effectiveness of the new kernel, extensive simulations have been carried out by employing this kernel in some well-known nonlinear diffusion filters. It has been shown that, at the expense of some increase in the processing time, the use of the proposed kernel in the nonlinear diffusion filters not only provides improved FOM values but also enhances their noise reduction capability.

Chapter 4

Nonlinear Diffusion Filtering for Poisson Noise Removal

4.1 Introduction

Performance of nonlinear diffusion filters, in terms of their noise removal and edge preservation capabilities, is intimeately related to the diffusion functions and the associated contrast parameters used by the filters. Furthermore, these nonlinear techniques do not perform well when the noise corrupting the images being denoised is non-stationary and signal-dependent. In this chapter, a nonlinear diffusion-based technique for denoising of images corrupted by Poisson noise is developed [98]. Starting from a Skellam distribution model for the gradient of the Poisson noise corrupted image and conducting a systematic investigation of the underlying diffusion mechanism, a spatially and temporally varying contrast parameter is designed. The nonlinear diffusion filter employing the contrast parameter thus designed is shown to satisfy the scale-space properties. Through a comprehensive simulation study, it is shown that the performance of the proposed technique, in terms of Poisson noise removal and edge preservation, is significantly superior to those of some the recent state-of-the-art techniques.

4.2 Role of Contrast Parameter in Nonlinear Diffusion Filter

A discrete realization of the nonlinear diffusion filter introduced by Perona and Malik [35] for processing a noisy digital image f in which each pixel position is indexed by (i, j), $i = 1, \cdots, I$; $j = 1, \cdots, J$, is given by

$$\begin{aligned} u_{i,j}^{(n+1)} &= u_{i,j}^{(n)} + \tau \sum_{d \in D} [g(\nabla_d u) \nabla_d u]_{i,j}^{(n)} \\ u^{(1)} &= f \ , \end{aligned} \tag{4.1}$$

where n is the iteration number, τ is a time step-size, $g(.)$ is a diffusivity function, and ∇_d is the directional derivative in the direction $d \in D = \{N, S, E, W\}$, i.e., in the direction north (N), south (S), east (E) or west (W), approximated as the difference of the pixel value $u_{i,j}$ and that of the nearest pixel in one of the four directions. Perona and Malik have introduced the following two expressions for the diffusivity function [35]:

$$g(\nabla_d u, K) = \frac{1}{1 + (|\nabla_d u|/K)^2} \tag{4.2}$$

$$g(\nabla_d u, K) = \exp - (|\nabla_d u|/2K)^2 \ , \tag{4.3}$$

where K is a tunning contrast parameter that controls the trade-off between the noise removing and edge preserving capabilities of the filter. In fact, the nonlinear diffusion filter using using either of these two diffusivity functions performs a strong forward diffusion in regions of the image u with $|\nabla_d u| \leq K$, and a reduced diffusion or even an inverse diffusion in regions when $|\nabla_d u| > K$. Therefore, a good choice of this contrast parameter in a nonlinear diffusion filter is the one that assumes a value larger than the gradient magnitude at pixels that are in the smooth regions of the image and it is smaller than that at the edge pixels. However, finding such a K is not a trivial task, since the gradient magnitude alone cannot distinguish between a noisy pixel and an edge pixel, specially when the noise level is high.

For finding a suitable K when the image is corrupted by an additive white Gaussian noise (AWGN), Perona and Malik [35] have suggested the use of an empirically obtained distribution function of the gradient magnitude, where the value of K at each iteration is set to be $80\% \sim 90\%$ of the value of the integral of the histogram of the absolute value of the gradient throughout the image. In [44], a technique based on using median absolute deviation was introduced for estimating the contrast parameter as

$$K = 1.4862 \times MAD(\nabla u) \,, \tag{4.4}$$

where $MAD(.)$ is defined as

$$MAD(\nabla u) = median(|\nabla u - median(|\nabla u|)) \,. \tag{4.5}$$

In contrast to the gradient based techniques of [35] and [44] for estimating a suitable contrast parameter, in [99] this parameter is estimated by using directly the variance of the contaminating AWGN. All these methods have resulted in a contrast parameter that is spatially invariant when the contaminating noise is specifically stationary uncorrelated AWGN. It should, however, be pointed out that in [2] a technique that provides a spatially-varying K has been developed and it is shown to provide improved performance for images with stationary AWGN contamination.

Development of spatially-varying contrast parameters for filtering of non-stationary noise has been a subject of intense research [38, 39, 99, 100]. However, the computational cost associated with these techniques of estimating a contrast parameter is high, since the value of K at each pixel position needs to be calculated by processing the noisy image in a small window centered at the pixel position. In this context, a constrained variational filter [101] has been developed for removing Poisson noise in which a spatially varying parameter set to be inversely proportional to the intensity of the diffusing image is used to control the trade-off between the noise removal and edge preservation capabilities of the filter. In this method, while the setting of the

parameter controlling the noise removal and edge preservation is greatly simplified, the optimization-based filtering process itself is very slow due to non-smoothness of the underlining cost function. Recent research efforts in this area have been focusing on finding the ways and means to improve the convergence rate of the optimization process [56–61]. In the next section, we develop an efficient technique for estimating a spatially varying contrast parameter in the framework of the rapidly convergent nonlinear diffusion filtering scheme of Perona and Malik [35] for the removal of Poisson noise.

4.3 Proposed Method

In this section, we develop the proposed technique for estimating a spatially and temporally varying contrast parameter K for an efficient filtering of the images contaminated with Poisson noise using the Perona-Malik nonlinear diffusion filter [35]. To this end, we first provide an initial estimate of K by modeling the gradient ∇_d of the piecewise smooth regions of an image contaminated with Poisson noise using Skellam distribution [102]. This initial estimate for K is then further modified to take into consideration the image singularities caused by the edges. The contrast parameter is finally modified to control the temporal diffusion of the image. The scale-space properties of the diffusion filter are studied in the context of this newly designed contrast parameter.

4.3.1 Initial Estimate of the Contrast Parameter using Skellam Distribution

For simplicity of notations, in the following we denote the pixel position (i, j) by a single index s and that of its immediate neighboring pixel in the direction d by d.

The pixel f_s of a given contaminated image f has a Poisson distribution:

$$f_s \sim \mathcal{P}(\mu = f_s^*) \ , \tag{4.6}$$

where f_s^* is the pixel value at (i, j) of the noiseless image f^*. If the pixel values of the noisy image f are assumed to be independent, then the distribution of $\nabla_d f_s$ is known to follow a Skellam distribution [102] given by

$$\nabla_d f_s \sim \mathcal{S}(mean = f_d^* - f_s^*, variance = f_d^* + f_s^*) \ . \tag{4.7}$$

Although this distribution model is based on the assumption that pixels of the noisy image are independent, it has been shown in [103] that, in practice, this model is sufficiently accurate to model the distribution of $\nabla_d f_s$.

Let us consider the image f^* to be a piecewise constant image (i.e., the noiseless image f^* consists of flat regions separated by step edges). In this case the distribution of $\nabla_d f_s$ at a pixel position $s \in R_i$, where R_i is a region of f corresponding to a flat region R_i^* of noiseless image f^*, becomes

$$\nabla_d f_s \sim \mathcal{S}(mean = 0, variance = f_d^* + f_s^*) \quad \forall \ f_s^*, \ f_d^* \in R_i^* \ , \tag{4.8}$$

with the probability density function being

$$p(x) = e^{(-2f_s^*)} I_{|x|}(2f_s^*) \ , \tag{4.9}$$

where $I_{|x|}$ is a modified Bessel function of the first kind. Assuming that X_i is the largest value of the $|\nabla_d f_s|$ in R_i, a suitable value of the contrast parameter K can be chosen as $K \geq X_i$ in order to remove the noise from the region R_i. However, it is practically not feasible to determine X_i, since it is not possible to specify the region R_i in f. On the other hand, the distribution of $\nabla_d f_s$ given by (4.8) provides us with some measure of the degree of the variability around its mean value of zero. Hence, we propose an initial estimate of K to be determined using this variability, as

$$K_s^d = \chi \sqrt{f_s^* + f_d^*} \ , \tag{4.10}$$

where χ is a spatially constant scaling coefficient. Note that the expression for the contrast parameter becomes $K_s^d = \chi\sqrt{2f_s^*}$, if $s \in R_i^*$. With this choice of the contrast parameter, we can compute the probability of $K_s^d \geq |\nabla_d f_s|$ in the region R_i, by using the probability density function given by (4.9), as

$$P(f_s^*) = \int_{-\chi\sqrt{2f_s^*}}^{\chi\sqrt{2f_s^*}} p(x)dx \ . \tag{4.11}$$

We now evaluate this probability using the built-in function for modified Bessel function of the first kind available in Matlab for $\chi = 0.35, 0.70, 1.0$ and 3 and f_s in the range $[1, 100]$. The results are depicted in Figure 4.1. It is seen from this figure that, except for a region R_i for which the corresponding region R_i^* in f^* has a very low intensity, $P(f_s^*)$ is almost independent of f_s^* and that it varies from a value of 0.27 to a value of almost unity as the value of χ is increased from 0.35 to 3. That is to say that the percentage of the pixel positions in R_i at which the condition $K \geq |\nabla_s f_s|$ is satisfied varies from 27% to almost 100% as χ is varied in the range $[0.35, 3]$.

Note that we have proposed an expression for the contrast parameter given by (4.10) for the removal of the noise only in the region R_i. However, before performing an experiment to examine its noise removal capability in R_i and to observe its impact on the diffusion of the edges (that is, when the filtering process is moved beyond the region R_i), we are faced with a practical problem, in that the expression given by (4.10) requires the knowledge of the noise-free image f^* corresponding to f. To overcome this problem, we propose to use the pixel values of the diffusing image u instead of those of f^* in the evaluation of the contrast parameter, as

$$K_s^{d^{(n)}} = \chi\sqrt{u_s^{(n)} + u_d^{(n)}} \ . \tag{4.12}$$

We now examine the impact of this modification in the contrast parameter. In order to study this impact, we conduct the following experiment. We choose the image *House* and corrupt it using the noise model given in (4.6). The noisy image is diffused by the nonlinear diffusion filter (4.1) with the diffusivity function given by (4.2) and τ

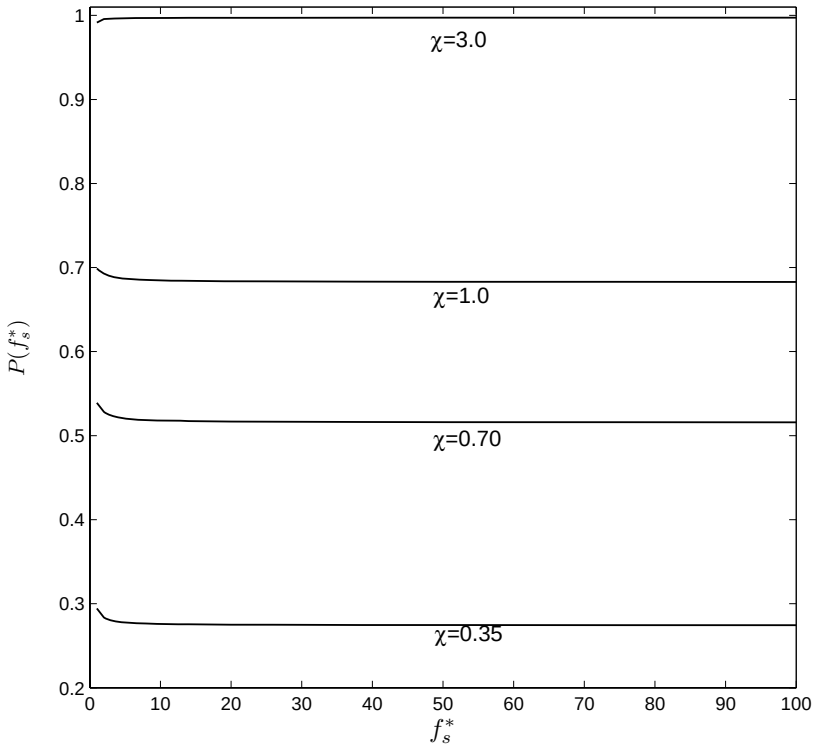

Figure 4.1: Evaluation of $P(f_s^*)$ given in (4.11) for $f_s^* \in [1, 100]$ and $\chi = 0.35, 0.70$, 1.0 and 3.0

set to be 0.2. For this diffusion process, we obtain the mean square difference (MSD) between the values of contrast parameter K_s^N using the expressions given by (4.10) and (4.12) as a function of the iteration number n for $\chi = 0.35$, 0.7, 1.0 and 3. The results are shown in Figure 4.2, from which it is seen that the initial difference between the values obtained using (4.10) and (4.12) is larger for larger value of χ. However, regardless of the value of χ, the difference becomes quite small as the diffusion is continued beyond $n = 10$ iterations.

With the expression for the contrast parameter now modified to a practically implementable form as given by (4.12) and the impact of this modification studied, we now examine the visual quality of the images in terms of noise removal and edge preservation capability of the nonlinear diffusion filter using this modified contrast

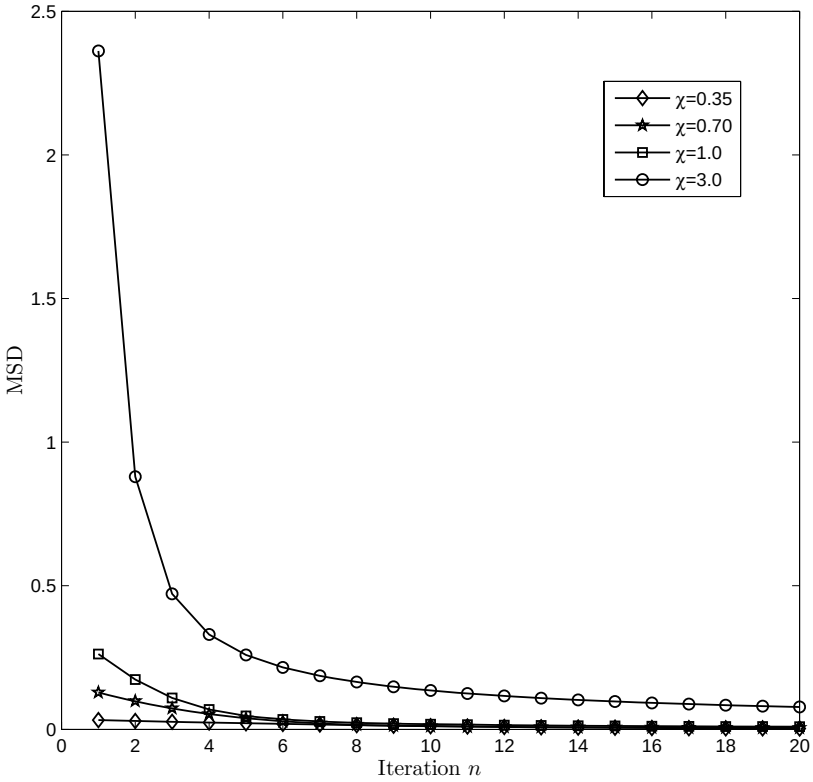

Figure 4.2: Mean square difference between the values of the contrast parameter evaluated using (4.10) and (4.12) as a function of iteration number.

parameter. Figures 4.3(a) and (b) show the original noiseless and Poisson noise corrupted *House* images, whereas, Figures 4.3(c), (d) and (e) show the images obtained by filtering the the image of Figures 4.3(b) using the contrast parameter given by (4.12) with the values of χ chosen as $0.35, 0.70$ and 3.0, respectively, after 20 iterations. It is seen that as the value of χ is increased from 0.35 to 3.0, more and more of the Poisson noise is removed at the expense of increasingly diffused edges. For $\chi = 0.35$, the edges are reasonably well preserved, but the noise is still visible in the image, whereas for $\chi = 3$ the noise is completely filtered out, but the edges are much diffused. In this example of filtering the *House* image, $\chi = 0.70$ seems to provide a good compromise between the noise removal and edge preservation capabilities of the nonlinear diffusion filter, as seen from Figure 4.3(d).

Finally, we conclude that a reasonable choice for the value of χ (for example

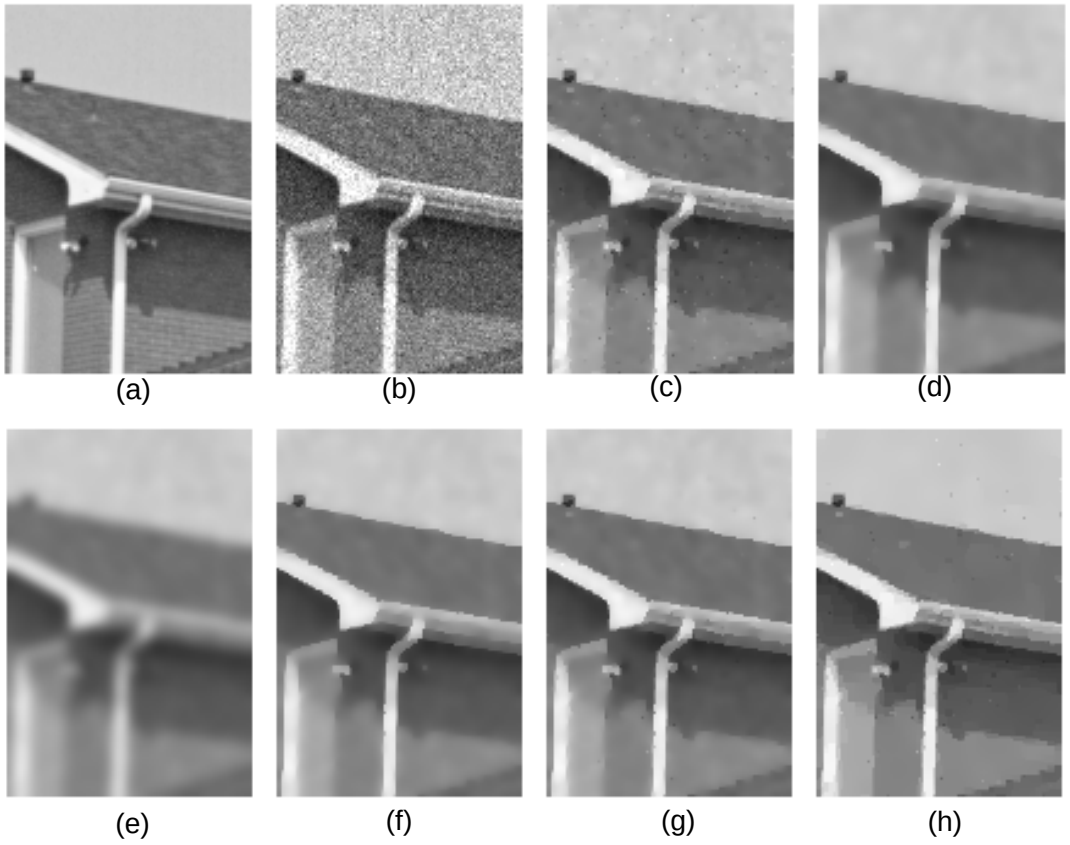

Figure 4.3: Comparing the perceptual quality of the denoised images obtained by nonlinear diffusion filter (4.1) using the diffusivity function given by (4.2). (a) Noiseless image; (b) Noisy image; (c)-(e) Denoised images where the contrast parameter is given by (4.12) with $\chi = 0.35$, 0.70 and 3.0, respectively; (f) Denoised image obtained by using the contrast parameter given by (4.18) with $\chi = 0.7$;(h) Denoised image obtained by using the contrast parameter given by (4.24) with $\chi = 0.70$; Denoised image obtained by using the proposed contrast parameter given in (4.28).

$\chi \geq 0.7$ in the above example) in the contrast parameter given by (4.12) can effectively remove the noise from all regions of the image f for which the corresponding regions in the noiseless image f^* are flat. In the next subsection, we modify the contrast parameter given by (4.12) by focusing on the pixel-dependent component, namely $\sqrt{u_s^{(n)} + u_d^{(n)}}$, of the contrast parameter in order to control the diffusion of the edges while still effectively removing the noise.

4.3.2 An Edge-Adaptive Contrast Parameter

In this section, we suitably modify the data dependent part $\sqrt{u_s^{(n)} + u_d^{(n)}}$ of the contrast parameter given by (4.12) so that its value on the edge pixels of the image gets reduced. As mentioned in Section II, if at edge pixels the contrast parameter is made to satisfy the condition

$$K < |\nabla_d u_s| = |u_d - u_s| \,, \tag{4.13}$$

then the pixels in question will have reduced diffusion or may undergo even an inverse diffusion. Satisfying the condition (4.13) at a pixel lying on an edge in image u, leads to the preservation or enhancement of the edge pixel during the filtering process. Using in (4.13) the expression for the contrast parameter given by (4.12), we have

$$|u_d - u_s| > \chi\sqrt{u_s + u_d} \,. \tag{4.14}$$

Solving the equation $|u_d - u_s| = \chi\sqrt{u_s + u_d}$ for u_d yields

$$u_d = \begin{cases} f_1(u_s) = \dfrac{2u_s + \chi^2 + \chi\sqrt{8u_s + \chi^2}}{2} \,, & \text{for } u_s < u_d \qquad (4.15) \\ f_2(u_s) = \dfrac{2u_s + \chi^2 - \chi\sqrt{8u_s + \chi^2}}{2} \,, & \text{for } u_s > u_d \,. \qquad (4.16) \end{cases}$$

The results of the above analysis is depicted in Figure 4.4(a) for $\chi = 1$ and u_s in the range $[0.05,\ 10]$. From the plot of the functions $u_d = f_1(u_s)$ and $u_d = f_2(u_s)$ as given by (4.15), the first quadrant of $u_s u_d$-plane gets divided into regions $\mathcal{R}_1$, $\mathcal{R}_2$ and $\mathcal{R}_3$. It is obvious from this figure that for an edge pixel u_s for which (u_s, u_d) lies in the region $\mathcal{R}_1$ or $\mathcal{R}_3$, the contrast parameter given by (4.12) will satisfy the condition given by (4.14). However, for an edge pixel u_s for which (u_s, u_d) lies in the region $\mathcal{R}_2$, this condition will be violated. Therefore, by using the contrast parameter given by (4.12), the edge pixels for which (u_s, u_d) lies in the region $\mathcal{R}_1$ or $\mathcal{R}_3$ will undergo a diffusion process in the direction $\vec{sd}$ at a rate that is smaller than when (u_s, u_d) lies in the region $\mathcal{R}_2$. We, therefore, conclude that a choice of the contrast parameter given in (4.12) is detrimental to preserving the edge pixels u_s such that $(u_s, u_d) \in \mathcal{R}_2$

under the diffusion process given by (4.1). Hence, our objective in any modification in the contrast parameter of (4.12) must focus on reducing the difference between the function $f_1(u_s)$ and $f_2(u_s)$, that is, to reduce the vertical depth of the region $\mathcal{R}_2$. The vertical depth of the region $\mathcal{R}_2$ can be obtained using (4.15) as

$$D_1(u_s) = f_1(u_s) - f_2(u_s) = \chi\sqrt{8u_s + \chi^2}\,. \tag{4.17}$$

Let us now modify the contrast parameter given by (4.12) as

$$K_s^d = \chi\sqrt{2min(u_s^{(n)}, u_d^{(n)})}\,. \tag{4.18}$$

Since in a region of u corresponding to R_i in f, $u_s^{(n)} \approx u_d^{(n)}$, we have $2min(u_s^{(n)}, u_d^{(n)}) \approx u_s^{(n)} + u_d^{(n)}$. Therefore, in this region, the modified contrast parameter given by (4.18) assumes approximately the same value as that assumed by (4.12). However, the intensity of an edge pixel u_s is substantially different from that of u_d. Therefore, for an edge pixel u_s, $2min(u_s^{(n)}, u_d^{(n)}) < u_s^{(n)} + u_d^{(n)}$, meaning that at an edge pixel u_s, the value of the contrast parameter given by (4.18) is lower than that obtained by using (4.12). Accordingly, the performance of the filter can be expected to improve in reducing the diffusion of the edges while retaining the same performance as that by using (4.12) in removing the noise in flat regions.

Using this modified contrast parameter, the condition (4.13) becomes

$$|u_d - u_s| > \begin{cases} \chi\sqrt{2u_s}\,, & \text{for } u_s < u_d \qquad (4.19) \\ \chi\sqrt{2u_d}\,, & \text{for } u_s > u_d\,. \qquad (4.20) \end{cases}$$

In a way similar to the previous case, we can determine the regions in $u_s u_d$-plane in which the condition given by (4.19) is satisfied by making use of the following functions:

$$u_d = \begin{cases} f_3(u_s) = u_s + \chi\sqrt{2u_s} & \text{for } u_s < u_d \qquad (4.21) \\ f_4(u_s) = \dfrac{2u_s + 2\chi^2 - \chi\sqrt{8u_s + 4\chi^2}}{2} & \text{for } u_s > u_d\,. \qquad (4.22) \end{cases}$$

The results for $\chi = 1$ and $u_s \in [0.05, 10]$ are depicted in Figure 4.4(b). It is seen from this figure that with the modification of the contrast parameter as in (4.18), the

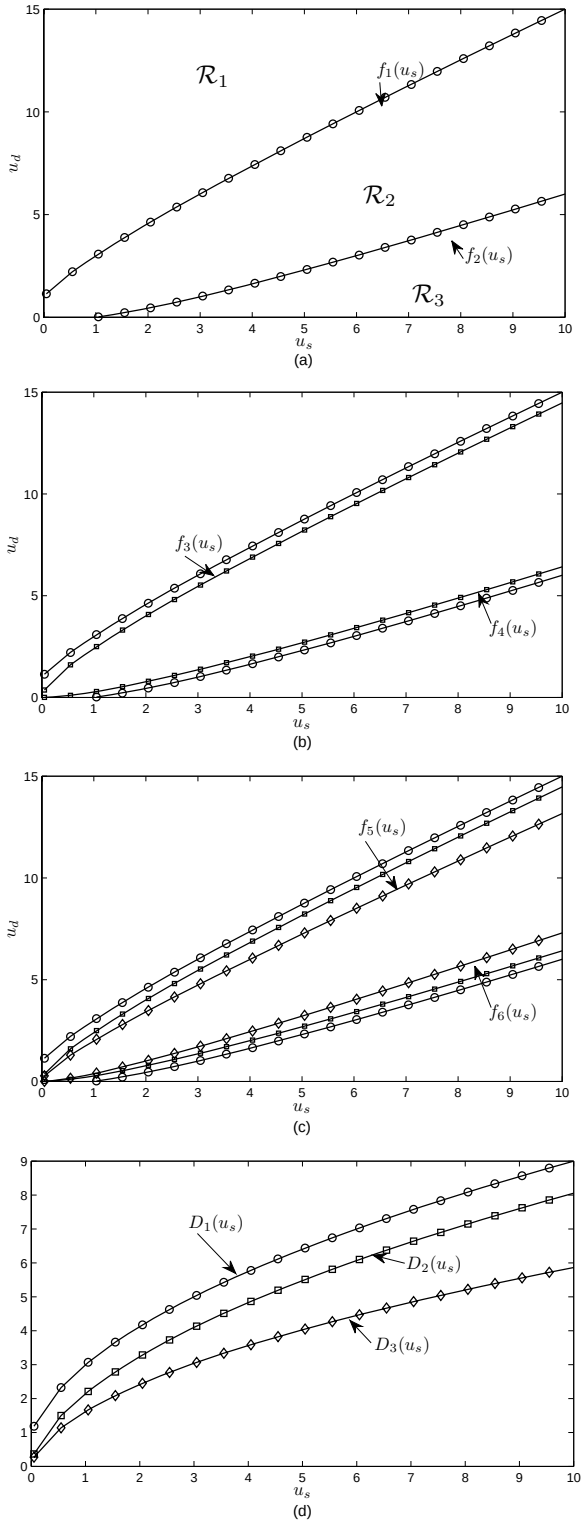

Figure 4.4: Impact of using the contrast parameters resulting from its various developmental stages. Illustration of the regions $\mathcal{R}_\infty$, $\mathcal{R}_\in$, $\mathcal{R}_\ni$ by using (a) (4.12), (b) (4.18) and (c) (4.24). (d) The vertical depth of the region $\mathcal{R}_\in$.

region $\mathcal{R}_2$ is vertically shrunk, that is, with the use of contrast parameter (4.18), the condition $K < |\nabla_d u_s|$ holds at an edge pixel u_s with smaller values of $|u_s - u_d|$ than that in the case of using the contrast parameter of (4.12). Thus, the use of contrast parameter (4.18) should enable to preserve edges with a smaller contrast. In this case, the vertical depth of the region $\mathcal{R}_2$ is given by

$$D_2(u_s) = f_3(u_s) - f_4(u_s) = \chi(\sqrt{2u_s + \chi^2} + \sqrt{2u_s}) - \chi^2 \ . \tag{4.23}$$

In order to see the visual performance of filter (4.1) using this modified contrast parameter given by (4.18), we again consider the noisy image *House* shown in Figure 4.3(b) and let it undergo the nonlinear diffusion process of (4.1) using the contrast parameter given by (4.18) with $\chi = 0.70$. The filtered image is shown in Figure 4.3(f). A comparison of the filtered images of Figures 4.3(d) and (f) shows that the edge preservation capability of the filter using (4.18) is improved over that using (4.12) while still removing the noise effectively.

In an effort to further decrease the value of the contrast parameter at edge pixels while keeping its value about the same in non-edge-pixel regions, we make use of the diffusivity function $g(.)$. Note that the value of $g(.)$ ranges between zero at edge pixels and unity at pixels in R_i. Thus, if the contrast parameter is modified as

$$\begin{aligned} K_s^{d^{(n)}} &= \chi\sqrt{[1 + g^{(n-1)}(.)]\, min(u_s^{(n)}, u_d^{(n)})} \\ g^{(0)}(.) &= 0 \ , \end{aligned} \tag{4.24}$$

its value will range between $\chi\sqrt{min(u_s, u_d)}$ at edge pixels and $\chi\sqrt{2min(u_s, u_d)}$ at pixels positions in R_i, i.e., the range of K_s^d becomes $[\chi\sqrt{min(u_s, u_d)}, \chi\sqrt{2u_s)}]$. Most of the diffusivity functions are designed so as to assume very small values at edge pixels. Therefore, in order to examine the ability of the contrast parameter given by (4.24) in further shrinking the region $\mathcal{R}_2$ vertically, we assume that $g^{(n-1)}(.)$ takes a value of zero at edge pixels. With this assumption, the functions separating the

regions $\mathcal{R}_1$ and $\mathcal{R}_2$ and regions $\mathcal{R}_2$ and $\mathcal{R}_3$ in the $u_s u_d$-plane are given by

$$u_d = \begin{cases} f_5(u_s) = u_s + \chi\sqrt{u_s}\,, & \text{for } u_s < u_s \qquad (4.25) \\ f_6(u_s) = \dfrac{2u_s + \chi^2 - \chi\sqrt{4u_s + \chi^2}}{2}\,, & \text{for } u_s > u_d\,. \qquad (4.26) \end{cases}$$

These functions, along with those obtained in connection with contrast parameters (4.12) and (4.18), are plotted in Figure 4.4(c). It is seen from this figure that the contrast parameter given by (4.24) has indeed succeeded in shrinking the region $\mathcal{R}_2$ further. The difference of the function $f_5(.)$ and $f_6(.)$ is given by

$$D_3(u_s) = \chi\left(\sqrt{u_s} + \sqrt{u_s + \chi^2/4}\right) - \frac{\chi^2}{2}\,. \qquad (4.27)$$

The difference functions $D_1(u_s), D_2(u_s)$ and $D_2(u_s)$ are plotted in Figure 4.4(d) in order to show as to how the contrast parameter given by (4.12), (4.18) and 4.24) have progressively shrunk the region $\mathcal{R}_2$.

Figure 4.3(g) shows the *House* image of Figure 4.3(b) filtered by using the contrast parameter given in (4.24). By comparing this image with that of Figure 4.3(f), it is seen that the filter with this contrast parameter is even more effective in preserving the edges without a loss in its ability to remove noise.

4.3.3 Temporal Curtailing of Diffusion

In the development of the contrast parameter in the proceeding sub-sections, the scaling coefficient χ was kept constant throughout the iterations. However, as seen in Section III.A, for a given noisy image, one needs to use a value of χ that provides an optimum performance in terms of the noise removal and edge preservation. We also know that during the initial phase of the iterations, the noise is predominant. Hence, during this phase, the use of large χ could be more effective for noise removal . But, keeping this same large value through the later phases of iterations would be detrimental to preserving the edges. Thus, by using the so-called threshold freezing mechanism [96], we finally modify the contrast parameter to make it temporally

decreasing:

$$\begin{aligned} K_s^{d^{(n)}} &= \chi^{(n)} \sqrt{\left[1 + g_d^{(n-1)}(.)\right] min(u_s^{(n)}, u_d^{(n)})} \\ g^{(0)}(.) &= 0 \\ \chi^{(n)} &= \chi_0/n \ , \end{aligned} \tag{4.28}$$

where χ_0 is a constant, which needs to be appropriately chosen. The use of contrast parameter of (4.28) will reduce the diffusion process through the iterations. Hence, the following condition can be used as a stopping criterion for further iterations

$$\frac{\sum_s (u_s^{(n)} - u_s^{(n-1)})^2}{\sum_s u_s^{(n)}} \leq T, \tag{4.29}$$

where T is a small positive number.

Figure 4.3(h) shows the image obtained by filtering the image of Figure 4.3(b) using the contrast parameter (4.28) with $\chi_0 = 2.38$. A comparison of this image with that in Figure 4.3(g) shows that the edge preservation capability of the filter using the final contrast parameter has increased over that using the contrast parameter given by (4.24).

4.3.4 Scale Space Properties

In this section, we study the scale-space properties of the nonlinear diffusion filter given by (4.1) when it employs the proposed contrast parameter of (4.28). It has been shown in [64] that if a nonlinear diffusion process expressed in the form

$$\begin{aligned} \mathbf{u}^{(n+1)} &= \mathbf{A}(\mathbf{u}^{(n)})\mathbf{u}^{(n)}, \ \ n = 1, 2, \cdots \\ \mathbf{u}^{(1)} &= \mathbf{f} \ , \end{aligned} \tag{4.30}$$

where $\mathbf{u} = (u_1, \cdots, u_s, \cdots, u_N)$ is a vector obtained by concatenating the columns of an image with u_s being a typical pixel value at position (i, j), N denotes the total

number of pixels in the image, and $\mathbf{A}$ is an $N \times N$ matrix with its $(k,l)th$ element denoted by $a_{k,l}$, satisfies the conditions:

(S1) $\sum_{l=1}^{N} a_{k,l} = 1$

(S2) $a_{k,l} = a_{l,k}$ $k, l \in \{1, \cdots, N\}$

(S3) continuity in the arguments of A, $A \in C(R^N, R^{N \times N})$

(S4) $a_{k,l} \geq 0$, $k, l \in \{1, \cdots, N\}$

(S5) $a_{k,k} > 0$, $k \in \{1, \cdots, N\}$

(S6) irreducibility of A for all $u \in R^N$

then the diffusion process maintains the scale-space properties. These conditions constitute a set of sufficient conditions to ensure that the diffusion process is well-posed and the output of the process converges to the a constant steady state and process supports the extremum principle and the property of average gray level invariance. It is seen that the nonlinear diffusion filter given by (4.1) is indeed expressible in the form given by (4.30) with the elements of the matrix A given by

$$a_{k,l} = \begin{cases} \tau g_{k,l}, & l \in N_d(k) \\ 1 - \tau \sum_{l \in N_d(k)} g_{kl}, & l = k \\ 0, & otherwise\ , \end{cases} \tag{4.31}$$

where $N_d(k)$ denotes the set of the indices of the immediate neighboring pixels of u_k in the 2-D image, and g_{kl} is the diffusion coefficient calculated using diffusion function (4.2) or (4.3) and the contrast parameter of (4.28) with $s = k$ and $d = l$. Before we verify that the nonlinear diffusion filter (4.1) employing the diffusivity function of (4.2) and the contrast parameter given by (4.28) satisfies the conditions (S1)-(S6), we prove the following lemma and theorem.

Lemma 1. *Elements of the matrix* **A** *satisfies*

$$\sum_{l=1}^{N} a_{k,l} = 1\,, \quad k \in \Omega = \{1, 2, \cdots, N\}\,. \tag{4.32}$$

Proof. We have

$$\sum_{l=1}^{N} a_{k,l} = \sum_{l \in N_d(k)} a_{k,l} + \sum_{l=k} a_{k,l} + \sum_{\substack{l=1 \\ l \neq k \\ l \notin N_d(k}}^{N} a_{k,l}\,,\ k \in \Omega\,. \tag{4.33}$$

Using (4.31) yields

$$\sum_{l=1}^{N} a_{k,l} = \sum_{l \in N_d(k)} \tau g_{k,l} + \left(1 - \sum_{l \in N_d(k)} \tau g_{k,l}\right) = 1\,,\ k \in \Omega\,. \tag{4.34}$$

□

Theorem 1. *If the the pixel values of a 2-D image f are strictly positive, i.e., $f = u^{(1)} \in \mathbb{R}^+$, $\chi_0 \neq 0$ and $0 < \tau < 0.25$, then for $n = 1, 2, \cdots$, the following holds:*

$$\begin{aligned} &(a) \qquad g_{k,l}^{(n)}(.) \text{ is a continuous function of } u_k^{(n)}, u_l^{(n)}, u_k^{(n-1)} \\ &\qquad\quad \text{and } u_k^{(n-1)} \text{ with its range given by } (0, 1] \\ &(b) \qquad f_{min} \leq u^{(n+1)} \leq f_{max}\,, \end{aligned}$$

where $f_{min} = \min\{f\}$ and $f_{max} = \max\{f\}$.

Proof. Depending on the relative values of $u_k^{(n)}$ and $u_l^{(n)}$, the diffusivity function (4.2) when it employs the contrast parameter given by (4.28), can be expressed as

$$g_{k,l}^{(n)}(u_k^{(n)}, u_l^{(n)}, g^{(n-1)}(.)) = \begin{cases} g_1^{(n)} = \frac{1}{1 + \frac{(u_l^{(n)} - u_k^{(n)})^2}{[\chi^{(n)}(1 + g^{(n-1)}(.))u_l^{(n)}]^2}}, & u_k^{(n)} > u_l^{(n)} \\ g_2^{(n)} = 1, & u_k^{(n)} = u_l^{(n)} \\ g_3^{(n)} = \frac{1}{1 + \frac{(u_l^{(n)} - u_k^{(n)})^2}{[\chi^{(n)}(1 + g^{(n-1)})(.)u_k^{(n)}]^2}}, & u_k^{(n)} < u_l^{(n)}\,. \end{cases} \tag{4.35}$$

We prove this theorem by induction.

(i) $n = 1$

Since $g^{(0)}(.) = 0$, for $n = 1$ (4.35) becomes

$$g_{k,l}^{(1)}(u_k^{(1)}, u_l^{(1)}, g^{(0)}(.)) = \begin{cases} g_1^{(1)} = \frac{1}{1+\frac{(u_l^{(1)}-u_k^{(1)})^2}{(\chi_0 u_l^{(1)})^2}}, & u_k^{(1)} > u_l^{(1)} \\ g_2^{(1)} = 1, & u_k^{(1)} = u_l^{(1)} \\ g_3^{(1)} = \frac{1}{1+\frac{(u_l^{(1)}-u_k^{(1)})^2}{(\chi_0 u_k^{(1)})^2}}, & u_k^{(1)} < u_l^{(1)} \ . \end{cases} \tag{4.36}$$

Since, $\chi_0 \neq 0$ and $u^{(1)} = f \in \mathbb{R}^+$, the functions $g_1^{(1)}$, $g_2^{(1)}$ and $g_3^{(1)}$, as given by (4.36), are defined and each is continuous function of $u_k^{(1)}$ and $u_l^{(1)}$ in the specified regions. Further, both $g_1^{(1)}$ and $g_3^{(1)}$ approach $g_2^{(1)}$ as $u_k^{(1)} \to u_l^{(1)}$, and $g_1^{(1)} = g_2^{(1)} = g_3^{(1)} = 1$ for $u_k = u_l$. Thus, $g^{(1)}(.)$ is a continuous function. Also, it is obvious from (4.36) that $g^{(1)}(.) \in (0, 1]$.

From (4.30), we have

$$u_k^{(2)} = \sum_{l \in \Omega} a_{k,l}^{(1)} u_l^{(1)}, \ k \in \Omega \ . \tag{4.37}$$

Since $0 < \tau < 0.25$ and the fact that $g^{(1)}(.) \in (0, 1]$, it is seen from (4.31) that all elements of $A(u^{(1)})$ are positive. Hence, by replacing $u_l^{(1)}$ in (4.37) with f_{min} and f_{max}, we have

$$\sum_{l \in \Omega} a_{k,l}^{(1)} f_{min} \leq u_k^{(2)} \leq \sum_{l \in \Omega} a_{k,l}^{(1)} f_{max} \ , \ k \in \Omega \ . \tag{4.38}$$

By factoring out f_{min} and f_{max} from the summations in (4.38), and since according *Lemma 1*, $\sum_{l \in \Omega} a_{k,l}^{(1)} = 1 \ \ \forall \ k \in \Omega$, we have

$$f_{min} \leq u_k^{(2)} \leq f_{max} \ , \ k \in \Omega \ . \tag{4.39}$$

This proves parts (a) and (b) of the theorem for $n = 1$.

(ii) $n = p$

Assume that (a) and (b) hold for $n = p$, that is,

$$g_{k,l}^{(p)}(.) \text{ is a continuous function of } u_k^{(p)}, u_l^{(p)}, u_k^{(p-1)} \text{ and } u_k^{(p-1)}, \text{ and } g_{k,l}^{(p)}(.) \in (0, 1] \tag{4.40a}$$

and

$$f_{min} \leq u^{(p+1)} \leq f_{max} \ . \tag{4.40a}$$

For $n = p + 1$, (4.35) can be written as

$$g_{k,l}^{(p+1)}(u_k^{(p+1)}, u_l^{(p+1)}, g^{(p)}(.)) = \begin{cases} g_1^{(p+1)} = \frac{1}{1+\frac{(u_l^{(p+1)} - u_k^{(p+1)})^2}{[\chi^{(p+1)}(1+g^{(p)}(.))u_l^{(p+1)}]^2}}, & u_k^{(p+1)} > u_l^{(p+1)} \\ g_2^{(p+1)} = 1, & u_k^{(p+1)} = u_l^{(p+1)} \\ g_3^{(p+1)} = \frac{1}{1+\frac{(u_l^{(n+1)} - u_k^{(n+1)})^2}{[\chi^{(p+1)}(1+g^{(p)})(.)u_k^{(p+1)}]^2}}, & u_k^{(p+1)} < u_l^{(p+1)} \ . \end{cases} \tag{4.41}$$

Using the condition given by (4.40a) and following the same reasoning as used to prove the theorem for $n = 1$, it easy to see that $g_{k,l}^{(p+1)}(.)$ is a continuous function with its range given by $(0, 1]$. In order to prove part (b) of the theorem for $n = p + 1$, we can write using (4.30)

$$u_k^{(p+2)} = \sum_{l \in \Omega} a_{k,l}^{(p+1)} u_l^{(p+1)} \ , \ k \in \Omega \ . \tag{4.42}$$

Using the above equation, and the fact $g_{k,l}^{(p+1)}(.) \in (0, 1]$ and $0 < \tau < 0.25$, we obtain the following inequalities:

$$\sum_{l \in \Omega} a_{k,l}^{(p+1)} u_{min}^{(p+1)} \leq u_k^{(p+2)} \leq \sum_{l \in \Omega} a_{k,l}^{(p+1)} u_{max}^{(p+1)} \ , \ k \in \Omega \ , \tag{4.43}$$

where $u_{min}^{(p+1)} = \min u_l^{(p+1)}$ and $u_{max}^{(p+1)} = \max u_l^{(p+1)} \ \forall \ l \in \Omega$. Using *Lemma 1* and (4.40), the above equation readily yields

$$f_{min} \leq u_k^{(p+2)} \leq f_{max} \ , \ k \in \Omega \ . \tag{4.44}$$

Thus, with the conditions given by (4.40), the theorem also holds for $n = p + 1$. □

Using the results of *Lemma 1* and *Theorem 1*, we now show that the nonlinear diffusion filter (4.1) using the diffusivity function given by (4.2) and the proposed

contrast parameter (4.28) satisfies the conditions (S1)-(S6). The condition (S1) is already proved as *Lemma 1*. In order for (S2) to hold, we must have $g_{k,l}^{(n)} = g_{l,k}^{(n)}$, which is equivalent to showing $K_s^{d(n)} = K_d^{s(n)}$. The proposed contrast parameter given by (4.28) indeed satisfies this last condition. According to (4.31), the continuity of the elements of $\mathbf{A}$, i.e., condition (S3), is dictated by the continuity of the function $g_{k,l}^{(n)}$, which is a result of *Theorem 1*. As for condition (S4), we have already established in the proof of *Theorem 1* that the $a_{k,l}$ elements of the matrix $\mathbf{A}$ are all positive. Condition (S5) is seen to be satisfied, since for $0 < \tau < 0.25$ and $g_{k,l} \in (0, 1]$, $a_{k,k}$ cannot be zero. As for condition (S6) , the necessary condition for the matrix $\mathbf{A}$ to be irreducible is given in [64]. A sufficient condition for $\mathbf{A}$ to be irreducible is that the elements $a_{k,k+1}$ and $a_{k,k-1}$ ($k \in \Omega$) are all non-zero. Using (4.31), it is easy to verify that in our case, where $0 < \tau < 0.25$ and $g_{k,l} \in (0, 1]$, these elements are strictly positive. Hence, A is irreducible.

Finally, it can easily be shown that if the nonlinear diffusion filter (4.1) employs the diffusivity function given by (4.3) along with the proposed contrast parameter (4.28), then *Lemma 1* and *Theorem 1* still applies and the diffusion filter satisfies conditions (S1)-(S6).

4.4 Simulation Results

In this section, we study the performance of the nonlinear diffusion filter given by (4.1) using the proposed contrast parameter for removing the Poisson noise and compare its performance with that of other state-of-the-art filters.

For our experiments, three test images, *Pepper*, *Cameraman* and *House*, are used. The size of these test images is 256×256 with the gray levels of the pixels lying in range of $[0, 255]$. In order to ensure the contaminated images to have low signal-to-noise ratio (SNR), the pixel values of each of the original images before its contamination

is scaled down by a factor so as to limit its maximum gray level in f_M^* to be 120, 60 or 30. The scaled down images are then contaminated according the noise model of (4.6) using a built-in function in MATLAB. In order to ensure that the filter (4.1) employing the proposed contrast parameter satisfies the scale space properties as well as to ensure that conditions of the filters used for comparison are also satisfied, the pixel values of the contaminated images smaller than $\epsilon = 10^{-15}$ are reset to ϵ.

The simulation of the nonlinear diffusion filter given by (4.1) using the diffusivity function of (4.2) in conjunction with the proposed contrast parameter requires setting the values of the parameters T and τ. We set $T = 10^{-4}$ and $\tau = 0.2$ in oder to ensure that iterative process achieves a good steady state. Gaussian kernel with variances of $0.30, 0.40$ and 0.50 are used in the diffusivity function given by (4.2) in order to provide spatial regularization for the processing of the contaminated images with $f_M^* = 120, 60$ and 30, respectively. As for setting the parameter χ_0, its optimum value is empirically obtained so as to satisfy the discrepancy principle for Poisson data [57], that is, an optimum value of χ_0 is obtained to result in a filtered image $\widehat{u}$ for which the expression

$$\frac{2}{I \times J} \sum_s \left(f_s \ln \frac{f_s}{\widehat{u}_s} + \widehat{u}_s - f_s \right) \tag{4.45}$$

approaches unity.

The performances of all the filters considered in this study are measured in terms of the peak signal-to-noise ratio (PSNR) representing the noise removal capability of the filters, and a figure of merit (FOM) index introduced in [11] that represents the edge preservation capability of the filters. The PSNR is defined as

$$PSNR = 10\, log_{10} \left(\frac{I \times J \times (f_M^*)}{\sum_s (f_s^* - \widehat{u}_s)^2} \right) , \tag{4.46}$$

where $\widehat{u}$ and f^* denote, respectively, the denoised and the noiseless images. The index

FOM, as defined in [11], is given by

$$FOM = \frac{1}{max\left(N_{\widehat{u}}, N_{\widehat{u}}\right)} \sum_{i=1}^{N_{\widehat{u}}} \frac{1}{1+\phi d_i^2} \,, \tag{4.47}$$

where $N_{\widehat{u}}$ is the number of detected edge pixels, N_{f^*} is the number of edge pixels in the original image f^*, ϕ is a positive scaling factor often chosen to be $1/9$, and d_i is the distance between the i^{th} detected edge pixel in $\widehat{u}$ and the corresponding pixel in f^*. For the evaluation of FOM, the *Sobel* operator is used for the edge detection.

All the filters in this section are implemented using a MATLAB 2008Ra simulation platform on a Windows-based 64-bit icore5 machine with 4-GB RAM.

The performance of the the proposed technique is compared with that of the state-of-the-art techniques presented in [61], [104] and [53] for Poisson noise removal. In our simulation of these three techniques, the parameter values used are the same as those reported in the respective publications. However, the optimal values for the parameters α and τ in the techniques of [61] and [104], respectively, which are used to control the trade-off between the noise reduction and edge preservation of the images, are determined empirically so as to provide the best values for the PSNR.

Table 4.1 gives the performance of the proposed filtering scheme and those of the other schemes mentioned above, in terms of PSNR and FOM of the denoised images, and the computational cost for processing the noisy images. It is seen from this table that amongst all the techniques considered, the proposed one provides with the best values for PSNR and FOM. For the three images, each with three different noise levels, the proposed technique, on the average, provides improvements of 9.18 dB in the PSNR over the average of the PSNR of the noisy images, which compares with the improvement of 7.13 dB, 7.53 dB and 8.53 dB provided by the TV-KL [61], SPIRAL-TV [104] and PURE-LET [53] filters, respectively. As regards the comparative performance of the filters in edge preservation, the proposed technique, on the average, provides improvements of 22.32%, 17.41% and 4.55% in the FOM values over those of the TV-KL, SPIRAL-TV, and PURE-LET techniques, respectively. In

regard to the computational times of the techniques, with the exception of the *Pepper* image with $f_M^* = 120$, the proposed technique has the lowest computational cost. On the average, the computational cost of the proposed technique is only 82%, 11.37% and 51% of that of the TV-KL, SPIRAL-TV, and PURE-LET techniques.

Table 4.1: Performance of various denoising filters

f_M^*	Noisy Image		Method	Optimal Values	Denoised Image		Time(s)
	Image	PSNR(dB)		of Parameters	PSNR(dB)	FOM	
120	*Pepper*	23.93	TV-KL [61]	$\alpha = 11$	28.97	0.8313	1.20
			SPIRAL-TV [104]	$\tau = 0.165$	29.32	0.7259	12.30
			PURE-LET [53]	–	30.89	0.8224	3.00
			Proposed	$\chi_0 = 1.78$	**31.29**	**0.8359**	**1.30**
	Cameraman	24.08	TV-KL [61]	$\alpha = 6.6$	28.81	0.7786	1.65
			SPIRAL-TV [104]	$\tau = 0.135$	29.13	0.7972	12.00
			PURE-LET [53]	–	30.40	0.9227	3.06
			Proposed	$\chi_0 = 1.25$	**30.49**	**0.9369**	**1.23**
	House	23.15	TV-KL [61]	$\alpha = 7.2$	31.13	0.7053	1.51
			SPIRAL-TV [104]	$\tau = 0.105$	31.26	0.7254	111.7
			PURE-LET [53]	–	31.32	0.8045	3.03
			Proposed	$\chi_0 = 1.47$	**32.38**	**0.8081**	**1.28**
60	*Pepper*	20.90	TV-KL [61]	$\alpha = 7$	27.00	0.6554	1.62
			SPIRAL-TV [104]	$\tau = 0.235$	28.27	0.6823	7.60
			PURE-LET [53]	–	29.15	0.7359	3.04
			Proposed	$\chi_0 = 1.49$	**29.89**	**0.7871**	**1.48**
	Cameraman	21.08	TV-KL [61]	$\alpha = 4.4$	27.27	0.7070	1.95
			SPIRAL-TV [104]	$\tau = 0.195$	27.37	0.7120	8.68
			PURE-LET [53]	–	28.57	0.8520	3.05
			Proposed	$\chi_0 = 1.13$	**28.80**	**0.8700**	**1.45**
	House	20.15	TV-KL [61]	$\alpha = 4.4$	29.43	0.6150	1.99
			SPIRAL-TV [104]	$\tau = 0.180$	29.44	0.6548	66.7
			PURE-LET [53]	–	30.11	0.6957	3.08
			Proposed	$\chi_0 = 1.44$	**31.05**	**0.7251**	**1.55**
30	*Pepper*	17.93	TV-KL [61]	$\alpha = 3.83$	25.18	0.5122	2.15
			SPIRAL-TV [104]	$\tau = 0.365$	26.13	0.6078	8.90
			PURE-LET [53]	–	27.46	0.6461	3.00
			Proposed	$\chi_0 = 1.37$	**28.39**	**0.7111**	**1.78**
	Cameraman	18.07	TV-KL [61]	$\alpha = 2.8$	25.33	0.6130	2.55
			SPIRAL-TV [104]	$\tau = 0.30$	25.73	0.6419	8.43
			PURE-LET [53]	–	26.94	0.7951	3.02
			Proposed	$\chi_0 = 1.02$	**27.20**	**0.8262**	1.74
	House	17.17	TV-KL [61]	$\alpha = 3.0$	27.59	0.5105	2.49
			SPIRAL-TV [104]	$\tau = 0.27$	27.60	0.5627	149.5
			PURE-LET [53]	–	28.43	0.6064	3.01
			Proposed	$\chi_0 = 1.31$	**29.61**	**0.6676**	**1.88**

For demonstrating the visual qualities of the images processed by the various filters considered, we choose the *Pepper* and *Cameraman* images as well as the image *Cell* available in the image processing tool-box of MATLAB. The images *Pepper* and *Cameraman* with $f_M^* = 30$ and the image *Cell* with $f_M^* = 60$ are contaminated to

have the PSNR values of 17.93 dB, 18.07 dB and 20.28 dB, respectively. The first two images shown in Figure 4.5, Figure 4.6 and Figure 4.7 are noiseless and noisy images, respectively. The images filtered by the TV-KL, SPIRAL-TV and PURE-LET techniques and by the proposed technique are depicted, respectively, as (c), (d), (e) and (f) in these figures.

An examination of the images in Figure 4.5 shows that the image in Figure 4.5(f) is visually better than that shown in Figure 4.5(c) and much better than the one in Figure 4.5(e) in terms of getting their noise removed. Also, the edges and textures in the image of Figure 4.5(f) are better preserved than that in Figure 4.5(d). A close look at the images in Figure 4.6 shows that image of Figure 4.6(f) portrays the best balance between the noise removal and edge preservation among all the denoised *Cameraman* images. Specifically, a comparison of the images in Figures 4.6(e) and (f) shows that the proposed method has removed the noise more effectively and has provided a better look of the *Cameraman*'s face. Further, the tower in the distant background is best preserved in the image Figure 4.6(f). It is also noted that in the image of Figure 4.6(c), one of the support of the tripod is completely distorted. From the filtered images depicted in Figures 4.7(c) and (d), it is clear that noise in the background is sufficiently removed; however, the texture on or near the boundary of the cells are blurred. In Figure 4.7(e), even though the fine details at the surface of cells are well preserved, the PURE-LET filter does not effectively remove the noise, particularly the noise surrounding the right cell. Figure 4.7(f) shows the result obtained by using the proposed filter, in which not only the noise has been effectively removed but also the fine details of the cells are better preserved in comparison to that in images obtained by using the other filtering schemes considered in this simulation study.

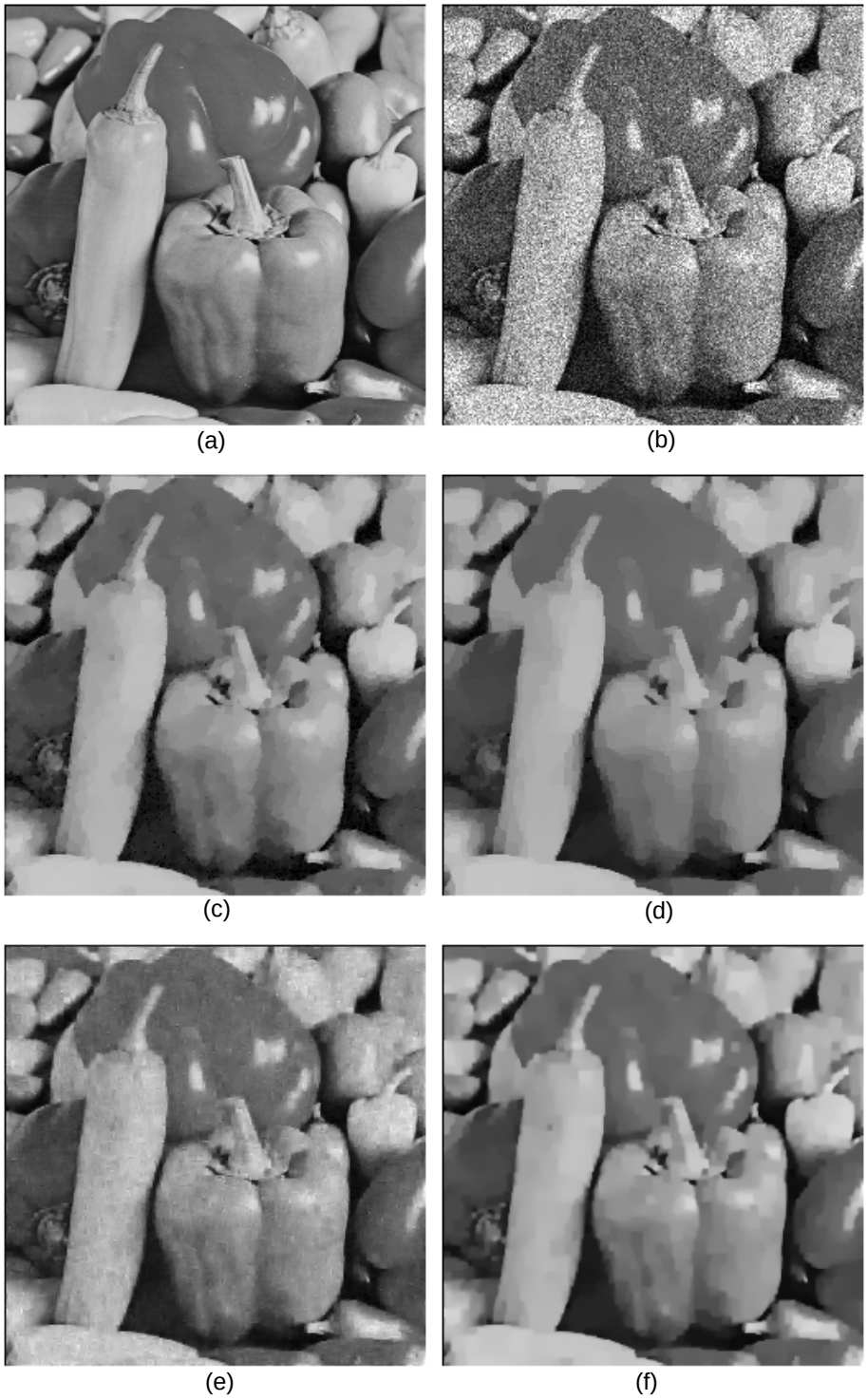

Figure 4.5: The perceptual quality of the processed image *Pepper*: (a) Noiseless image. (b) Noisy image when $f_M^* = 30$. (c) Image denoised using TV-KL with $\alpha = 3.83$. (d) Image denoised using SPIRAL-TV with $\tau = 0.365$. (e) Image denoised using PURE-LET. (f) Image denoised using proposed method with $\chi_0 = 1.37$.

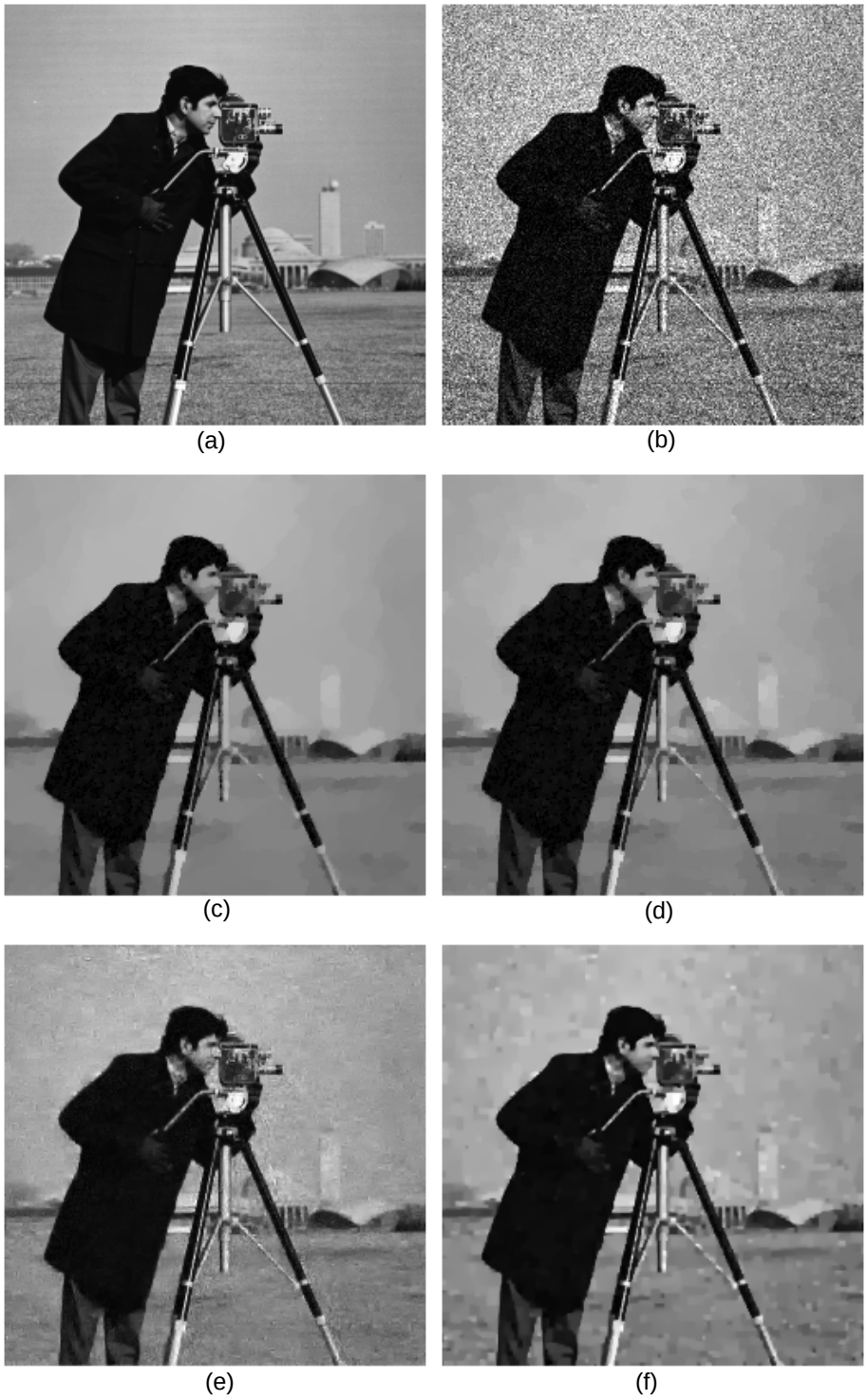

Figure 4.6: The perceptual quality of the processed image *Cameraman*: (a) Noiseless image. (b) Noisy image when $f_M^* = 30$. (c) Image denoised using TV-KL with $\alpha = 2.80$. (d) Image denoised using SPIRAL-TV with $\tau = 0.30$. (e) Image denoised using PURE-LET. (f) Image denoised using proposed method with $\chi_0 = 1.02$.

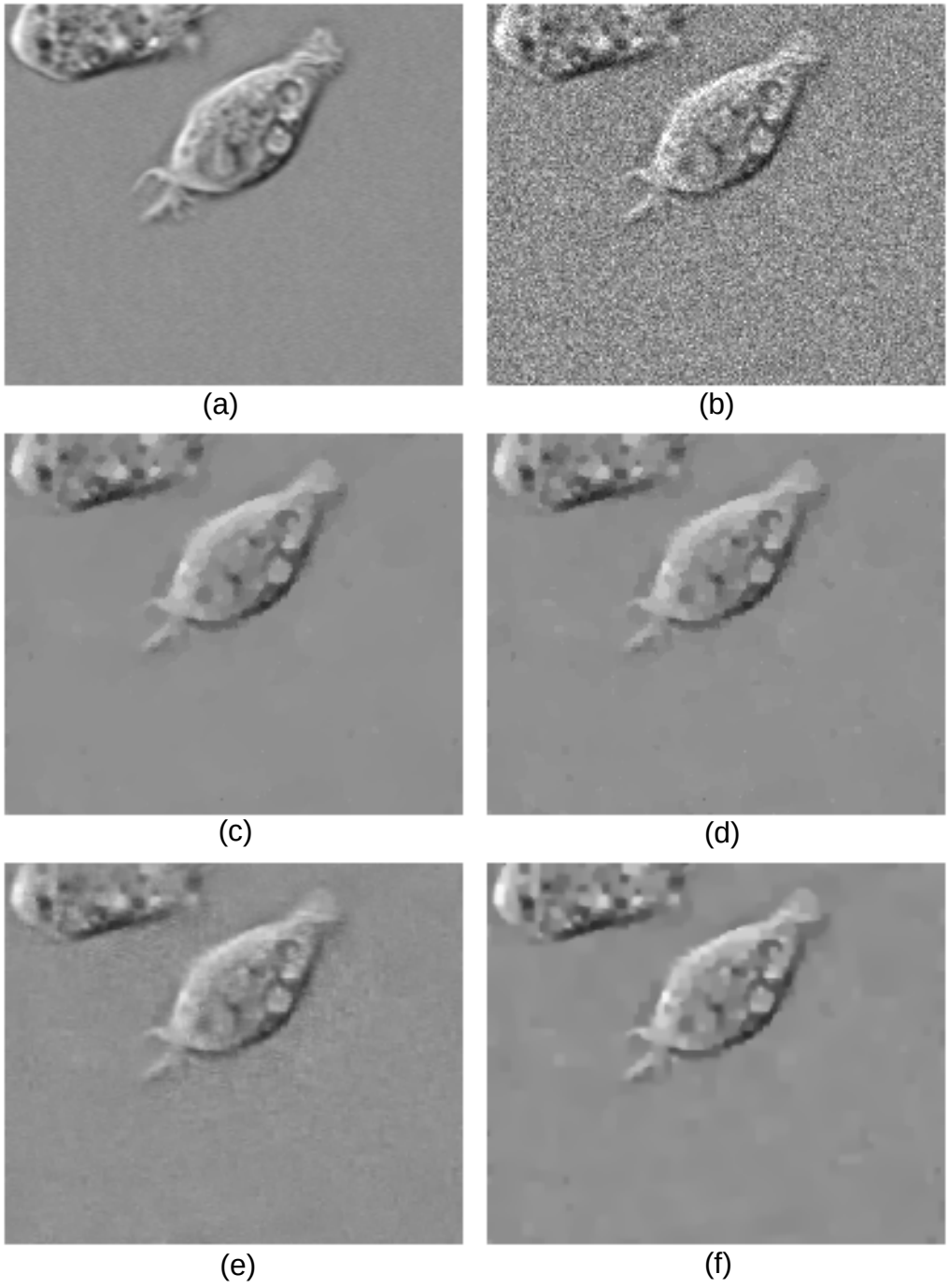

Figure 4.7: The perceptual quality of the processed image *Cell*: (a) Noiseless image. (b) Noisy image when $f_M^* = 60$. (c) Image denoised using TV-KL with $\alpha = 5.9$ ($PSNR = 31.54\ dB$ and $FOM = 0.4392$). (d) Image denoised using SPIRAL-TV with $\tau = 0.130$ ($PSNR = 31.41\ dB$ and $FOM = 0.4786$). (e) Image denoised using PURE-LET ($PSNR = 31.53\ dB$ and $FOM = 0.4474$). (f) Image denoised using the proposed method with $\chi_0 = 1.19$ ($PSNR = 32.43\ dB$ and $FOM = 0.5796$).

4.5 Summary

Performance of the techniques for noise removal, in which the diffusion process is modeled as a nonlinear partial differential equation, predominantly depends on the choice of the diffusion functions, specially on the ability of the associated contrast parameter, in removing the noise and preserving the edges of the image being denoised. The performance optimality of the denoising in these techniques is generally based on the assumption that noise and signal are uncorrelated. The photon-limited images in medical imaging systems and images in remote sensing are mainly degraded by Poisson noise having strong signal dependence, and they are examples of noise corruption in which the assumption of stationarity or uncorrelatedness of the contaminating noise for an optimal performance of the filter is no longer valid. In this chapter, a study has been undertaken to develop a technique for denoising of the images contaminated by Poisson noise within the framework of the Perona-Malik nonlinear diffusion filter. Starting from a Skellam distribution model of the gradient of a Poisson noise corrupted image and utilizing the mechanism of nonlinear diffusion process as it navigates spatially and temporally through the noise regions corresponding to the regions of the original image with and without edge pixels, a spatially and temporally varying contrast parameter has been designed. It has been shown that the nonlinear diffusion filter incorporating the proposed contrast parameter satisfies the scale-space properties. Extensive simulations have been performed to study the objective and subjective performances of the proposed and some of the other recently proposed techniques. The experimental results have demonstrated the superiority of the proposed technique in removing the noise and preserving the edges of the images contaminated by Poisson noise.

Chapter 5

Conclusion

5.1 Concluding Remarks

This thesis has been an investigation of the diffusion process of nonlinear diffusion filters as it concerns their capabilities for noise removal and edge preservation of images. The discretized versions of nonlinear differential equations modeling the diffusion process make use of kernels to perform the operations of spatial derivatives and contrast parameters to control the diffusion process. In this thesis, the roles of Laplacian kernels and contrast parameters have been investigated from standpoint of noise removal and edge preservation capabilities of the filters employing them. Based on this study, an edge-adaptive Laplacian kernel for removal of additive white Gaussian noise and a spatially and temporally varying contrast parameter for removal of Poisson noise from images have been developed.

In the first part of the thesis, a study has been first carried out to examine the impact of the anisotropic behavior of the Rosenfeld and Kak's Laplacian operator on the edge preservation capability of a discrete version of the Perona-Malik nonlinear diffusion filter. The result of this study has revealed that edges with different orientations having the same contrast can be diffused differently because of the anisotropic

behavior of this operator. This has motivated the development of a new Laplacian Kernel that when operating on pixels of orthogonal edges yields a zero response. It has been shown that even though the filter employing this kernel halts the diffusion process completely on orthogonal edges, the filter itself, in this case, does not satisfy the extremum principle. This problem has been analytically investigated to derive sufficient conditions for observance of the extremum principle and eventually to propose an edge-adaptive Laplacian kernel. The proposed Laplacian kernel has been used in different nonlinear diffusion filters, namely the Perona-Malik filter, the anisotropic filter of Carmona and Zhong and the gradient vector flow based anisotropic filter of Yu and Chua, in order to demonstrate its effectiveness in improving the filters' performance.

In the second part of the thesis, with a focus on the design of a new contrast parameter, a study has been undertaken to develop a technique for denoising images contaminated by Poisson noise within the framework of the Perona-Malik nonlinear diffusion filter. Starting from a Skellam distribution model of the gradient of a Poisson noise corrupted image and utilizing the mechanism of nonlinear diffusion process as it proceeds spatially and temporally through the regions of the image with and without edges, a spatially and temporally varying contrast parameter has been designed. It has been shown that the nonlinear diffusion filter incorporating the proposed contrast parameter satisfies the scale-space properties.

The effectiveness of the proposed techniques has been demonstrated by performing a set of comprehensive experiments using benchmark images. It has been shown that the edge preservation and noise reduction capabilities of the nonlinear diffusion filters employing the proposed Laplacian kernel are significantly improved when they are used for denoising images contaminated by additive white Gaussian noise, with some increase in the processing time. The effectiveness of the proposed contrast parameter has been shown by using it in the Perona-Malik filter and comparing the

results of denoising images with that of some recent state-of-the-art nonlinear filters. The subjective and objective evaluations of the performances of these filters have convincingly demonstrated the superiority of the proposed filtering technique in its noise removal and edge preservation capabilities and in the computational cost.

5.2 Scope for Future Work

The techniques of nonlinear diffusion proposed in this thesis have been developed to denoise gray-level images. A study could be undertaken for development of Laplacian operators and contrast parameters for nonlinear diffusion filters to denoise vector-valued images contaminated with different kinds of noise. The possibility of extending the proposed techniques to applications modeled with higher-order partial differential equations could be also explored. The impact of using the proposed Laplacian kernel and contrast parameter on image denoising by nonlinear diffusion filters employing diffusivity functions other than those considered in this thesis could also be investigated.

The techniques and schemes of this thesis to develop an edge-adaptive kernel and spatially and temporally varying contrast parameter for denoising of images using nonlinear partial differential equation based diffusion models could be further investigated for image processing applications such as deblurring and segmentations.

References

[1] J. T. Bushberg, J. A. Siebert, E. M. Leidholdt, and J. M. Boone, *The Essential Physics of Medical Imaging*. Baltimore: Williams and Wilkins, 2002.

[2] T. Rabie, "Robust estimation approach for blind denoising," *IEEE Transactions on Image Processing*, vol. 14, no. 11, pp. 1755–1765, Nov. 2005.

[3] J. Starck, F. Murtagh, and A. Bijaoui, *Image Processing and Data Analysis: the multiscale approach*. Cambridge: Cambridge University Press, 1998.

[4] H. H. Barrett and K. J. Myers, *Foundation of image science*. Hoboken, NJ: WILEY, 2004.

[5] R. Ferrari and R. Winso, "Digital radiographic image denoising via wavelet-based hidden Markov model estimation," *Journal of Digital Imaging*, vol. 18, no. 2, pp. 154–167, June 2005.

[6] C. M. Mukesh, C. G. Mukesh, C. M. Rakhi, and C. Frederick, "Survey of image denoising techniques," in *In Proceedings of Global Signal Processing Expo (GSPx)*, Santa Clara, CA., 2004, pp. 1–7.

[7] A. Buades, B. Coll, and J. Morel, "A review of image denoising algorithms, with a new one," *Multiscale Modeling and Simulation*, vol. 4, no. 2, pp. 490 – 530, 2005.

[8] T. F. Chan and J. Shen, *Image Processing and Analysis*. Philadelphia,PA: SIAM, 2005.

[9] K. Watson, "Processing remote sensing images using the 2-D FFT-noise reduction and other applications," *Geophysics*, vol. 58, no. 6, pp. 835–852, 1993.

[10] A. Foi, V. Katkovnik, and K. Egiazarian, "Pointwise shape-adaptive DCT for high-quality denoising and deblocking of grayscale and color images," *IEEE Transactions on Image Processing*, vol. 16, no. 5, pp. 1395 –1411, May 2007.

[11] W. Pratt, *Digital Image Processing.* New York: Wiley, 1977.

[12] A. Antoniadis, J. Bigot, and T. Sapatinas, "Wavelet estimators in nonparametric regression: A comparative simulation study," *Journal of Statistical Software*, vol. 6, no. 6, pp. 1–83, 2001.

[13] D. Donoho and Johnstone, "Ideal spatial adaptation by wavelet shrinkage," *Biometrika*, vol. 81, pp. 425–455, 1994.

[14] D. Donoho, "De-noising by soft-thresholding," *IEEE Trans. on Information Theory*, vol. 41, no. 3, pp. 613–627, 1995.

[15] K. Berkner and O. Wells, Raymond, "A correlation-dependent model for denoising via nonorthogonal wavelet transforms," Rice Univeristy Technical Report CML TR 98–07, Tech. Rep., 1998.

[16] J. Yinpeng, E. Angelini, and A. Laine, *Handbook of Biomedical Image Analysis*, ser. Handbook of Medical Image Analysis. New York: Springer US, 2004, ch. Wavelets in Medical Image Processing: De-noising, Segmentation, and Registration, pp. 304–359.

[17] A. Achim, P. Tsakalides, and A. Bezerianos, "SAR image denoising via bayesian wavelet shrinkage based on heavy-tailed modeling," *IEEE Transactions on Geoscience and Remote Sensing*, vol. 41, no. 8, pp. 1773–1784, 2003.

[18] E. P. Simoncelli and E. H. Adelson, "Noise removal via bayesian wavelet coring," in *Third IEEE Intl Conf. on Image Processing*, vol. 1, 1996, pp. 379–382.

[19] P. Moulin and J. Liu, "Analysis of multiresolution image denoising schemes using a generalized Gaussian and complexity priors," *IEEE Trans. Inform. Theory,*, vol. 45, pp. 909–919, 1999.

[20] S. M. M. Rahman, M. O. Ahmad, and M. N. S. Swamy, "Wavelet-based video denoising using Gauss-Hermite density function," in *49th IEEE International Midwest Symposium on Circuits and Systems MWSCAS,*, vol. 1, Aug. 2006, pp. 592 –595.

[21] ——, "Video denoising based on inter-frame statistical modeling of wavelet coefficients," *IEEE Transactions on Circuits and Systems for Video Technology*, vol. 17, no. 2, pp. 187–198, Feb 2007.

[22] ——, "Bayesian wavelet-based image denoising using the gausshermite expansion," *IEEE Transactions on Image Processing*, vol. 17, no. 10, pp. 1755–1771, Oct. 2008.

[23] N. Gupta, "Video modeling and noise reduction in wavelet domain," Ph.D. dissertation, Concordia University, November 2011.

[24] N. Gupta, M. Swamy, and E. Plotkin, "Despeckling of medical ultrasound images using data and rate adaptive lossy compression," *IEEE Transactions on Medical Imaging*, vol. 24, pp. 743–754, June 2005.

[25] D. Sen, M. Swamy, and M. Ahmad, "Unbiased homomorphic system and its application in reducing multiplicative noise," in *IEE Proc. Vision, Image and Signal Processing*, vol. 153, Oct. 2006, pp. 521–537.

[26] M. I. H. Bhuiyan, M. O. Ahmad, and M. N. S. Swamy, "Spatially-adaptive thresholding in wavelet domain for despeckling of ultrasound images," *IET Image Processing*, vol. 3, pp. 147–162, June 2009.

[27] ——, "Spatially adaptive wavelet-based methods using the cauchy prior for despeckling sar images," *IEEE Transactions on Circuits and Systems for Video Technology*, vol. 17, no. 4, pp. 500–507, April 2007.

[28] N. Kingsbury, "Image processing with complex wavelets," *Phil. Trans.Roy. Soc. London*, vol. 357, p. 25432560, 1999.

[29] D. Donoho and R. R. Coifman, Eds., *Translation-Invariant De-noisning.*, ser. In Wavelet and Statistics,. Springer-Verlag, 1995.

[30] M. Lang, H. Guo, J. E. Odegard, C. S. Burrus, and R. O. Wells, "Noise reduction using an undecimated discrete wavelet transform," *IEEE Signal Processing Letters*, vol. 3, no. 1, pp. 10–12, Jan. 1996.

[31] G. P. Nason and B. W. Silverman, "The stationary wavelet transform and some statistical applications," *Lecture Notes in Statistics: Wavelets and Statistics*, vol. 103, pp. 281–300, 1995.

[32] M. Fargues, R. Barsanti, R. Hippenstiel, and G. Coutu, "Wavelet-based denoising: comparisons between orthogonal and non-orthogonal decompositions," in *Proceedings of the 40th Midwest Symposium on Circuits and Systems*, vol. 2, 1997, pp. 929–932.

[33] Gonzalez and Woods, *Digital Image Processing,*. New Jersey: Printice-Hall, 2002.

[34] A. B. Hamza, P. L. Luque-Escamilla, J. Martinez-Aroza, and R. Roman-Roldan, "Removing noise and preserving details with relaxed median filters," *Journal of Mathematical Imaging and Vision*, vol. 11, no. 2, pp. 161–77, 1999.

[35] P. Perona and J. Malik, "Scale-space and edge detection using anisotropic diffusion," *IEEE Transactions on Pattern Analysis and Machine Intelligence*, vol. 12, no. 7, pp. 629–39, July 1990.

[36] L. Rudin, S. Osher, and E. Fatemi, "Nonlinear total variation based noise removal algorithms," *Physica D*, vol. 60, pp. 259–268, 1992.

[37] B. Li, N. Sang, Z. Cao, and T. Zhang, "Enhancement of X-ray angiogram images by adaptive anisotropic diffusion," *Electronics Letters*, vol. 41, no. 20, pp. 1107–1109, 2005, 0013-5194.

[38] G. Guido, O. Kabler, R. Kikinis, and F. A. Jolesz, "Nonlinear anisotropic filtering of MRI data," *IEEE Transactions on Medical Imaging*, vol. 11, no. 2, pp. 221–232, June 1992.

[39] J. S. Jin, Y. Wang, and J. Hiller, "An adaptive nonlinear diffusion algorithm for filtering medical images," *IEEE Transactions on Information Technology in Biomedicine*, vol. 4, no. 4, pp. 298–305, Dec. 2000.

[40] W. Wang, "Anisotropic diffusion filtering for reconstruction of Poisson noisy sinograms," *Journal of Communication and Computer*, vol. 2, no. 11, 2005.

[41] K. Hae Yong, J. Giacomantone, and C. Zang Hee, "Robust anisotropic diffusion to produce enhanced statistical parametric map from noisy fMRI," *Computer Vision and Image Understanding*, vol. 99, no. 3, pp. 435–452, 2005.

[42] H. M. Salinas and D. C. Fernández, "Comparison of PDE-based nonlinear diffusion approaches for image enhancement and denoising in optical coherence tomography," *IEEE Transactions on Medical Imaging*, vol. 26, no. 06, June 2007.

[43] M. Schaap, A. M. Schilham, K. J. Zuiderveld, M. Prokop, E.-J. Vonken, and W. J. Niessen, "Fast noise reduction in computed tomography for improved 3-D visualization," *IEEE Transactions on Medical Imaging*, vol. 27, no. 8, pp. 1120 – 1129, 2008.

[44] M. J. Black, G. Sapiro, D. H. Marimont, and D. Heeger, "Robust anisotropic diffusion," *IEEE Transactions on Image Processing*, vol. 7, no. 3, pp. 421–32, March 1998.

[45] Z. Lin and Q. Shi, "An anisotropic diffusion PDE for noise reduction and thin edge preservation," in *Proceedings of the 10th International Conference on Image Analysis and Processing*, Venice, Italy, 1999, pp. 102 –107.

[46] F. Anscombe, "The transformation of Poisson, binomial and negative-binomial data,," *Biometrics*, vol. 35, pp. 246–254, 1948.

[47] J. O. Deasy, "Denoising of electron beam Monte Carlo dose distributions using digital filtering techniques," *Phys. Med. Biol*, vol. 45, pp. 1765–1779, 2000.

[48] M. Jansen, "Multiscale Poisson data smoothing," *J. Royal Statistical Society*, vol. 68, no. 1, pp. 27–48, 2006.

[49] P. Frryzlewicz and G. Nason, "A Haar-Fisz algorithm for Poisson intensity estimation," *Journal of Computational and Graphical Statistics*, vol. 13, no. 3, pp. 621–638, March 2004.

[50] R. Nowak and E. Kolaczyk, "A statistical multiscale framework for Poisson inverse problems," *IEEE Transactions on Information Theory*, vol. 46, no. 5, pp. 1811 – 25, Aug. 2000. [Online]. Available: http://dx.doi.org/10.1109/18.857793

[51] S. Lefkimmiatis, P. Maragos, and G. Papandreou, "Bayesian inference on multiscale models for Poisson intensity estimation: Applications to photon-limited image denoising," *IEEE Transactions on Image Processing*, vol. 18, no. 8, pp. 1724 –1741, Aug. 2009.

[52] R. Willett and R. Nowak, "Multiscale Poisson intensity and density estimation," *IEEE Transactions on Information Theory*, vol. 53, no. 9, pp. 3171 –3187, Sept. 2007.

[53] F. Luisier, T. Blu, and M. Unser, "Image denoising in mixed Poisson-Gaussian noise," *IEEE Transactions on Image Processing*, vol. 20, no. 3, pp. 696 –708, March 2011.

[54] R. R. Berger, Jonathan; Coifman and M. J. Goldberg, "Removing noise from music using local trigonometric bases and wavelet packets," *J. Audio Eng. Soc*, vol. 42, no. 10, pp. 808–818, Oct. 1994.

[55] I. Csiszar, "Why least squares and maximum entropy? an axiomatic approach to inference for linear inverse problems," *The Annals of Statistics*, vol. 19(4), pp. 2032–2066, 1991.

[56] R. H. Chan and K. Chen, "Multilevel algorithm for a Poisson noise removal model with total-variation regularization," *Int. J. Comput. Math.*, vol. 84, no. 8, pp. 1183–1198, May 2007.

[57] R. Zanella, P. Boccacci, L. Zanni, and M. Bertero, "Efficient gradient projection methods for edge-preserving removal of Poisson noise," *Inverse Problems*, vol. 25, no. 4, pp. 045 010–+, Apr. 2009.

[58] M. Figueiredo and J. Bioucas-Dias, "Deconvolution of Poissonian images using variable splitting and augmented Lagrangian optimization," in *Proc. IEEE/SP 15th Workshop on Statistical Signal Processing*, Sept 2009, pp. 733 –736.

[59] S. Setzer, G. Steidl, and T. Teuber, "Deblurring Poissonian images by split Bregman techniques," *J. Vis. Comun. Image Represent.*, vol. 21, pp. 193–199, April 2010. [Online]. Available: http://dx.doi.org/10.1016/j.jvcir.2009.10.006

[60] R. Willett, Z. Harmany, and R. Marcia, "Poisson image reconstruction with total variation regularization," in *Proc. 17th IEEE International Conference on Image Processing (ICIP)*, Sept. 2010, pp. 4177 –4180.

[61] C. Wu, J. Zhang, and X.-C. Tai, "Augmented Lagrangian method for total variation restoration with non-quadratic fidelity," *Inverse Problems and Imaging*, vol. 5, no. 1, pp. 237 – 261, Feb. 2011.

[62] S. L. Keeling and R. Stollberger, "Nonlinear anisotropic diffusion filters for wide range edge sharpening," in *Proceedings of the International Society for Optical Engineering*, San Diego, 2000, pp. 1309–1322.

[63] ——, "Nonlinear anisotropic diffusion filtering for multiscale edge enhancement," *Inverse Problems*, vol. 18, no. 1, pp. 175 – 190, 2002. [Online]. Available: http://dx.doi.org/10.1088/0266-5611/18/1/312

[64] J. Weickert, *Anisotropic Diffusion in Image Processing.* Stuttgart: B. G. Teubner, 1998.

[65] S. K. Weeratunga and C. Kamath, "PDE-based nonlinear diffusion techniques for denoising scientific and industrial images: an empirical study," in *Image Processing: Algorithms and Systems*, vol. 4667, 2002, pp. 279–290.

[66] S. Kichenassamy, "Perona-Malik paradox," *SIAM Journal on Applied Mathematics*, vol. 57, no. 5, pp. 1328 – 1342, 1997.

[67] S. K. Weeratunga and C. Kamath, "Comparison of PDE-based non-linear anisotropic diffusion techniques for image denoising," in *Proceeding of SPIE*, vol. 5014, no. 201, Santa Clara,, Jan. 2003, pp. 201–212. [Online]. Available: http://dx.doi.org/10.1117/12.477744

[68] J. Koenderink, "The structure of images," *Biological Cybernetics*, vol. 50, pp. 363–370, 1984.

[69] A. Hummel, "Representation based on zero-crossing in scale-space," in *Proceedings of IEEE Cmputer Vision and Patern Recognition*, 1986, pp. 204–209.

[70] J. Weickert, "A review of nonlinear diffusion filtering," in *Scale-Space Theory in Computer Vision*, ser. Proceedings of First International Conference on Scale-Space, vol. 1252, Utrecht, Netherlands, 1997, pp. 3–28.

[71] Y. You, W. Xu, A. Tannenbaum, and M. Kaveh, "Behavioral analysis of anisotropc diffusion in image processing," *IEEE Transaction on Image Processing*, vol. 5, pp. 1539–1553, 1996.

[72] P. Charbonnier, G. Aubert, L. Feraud, and M. Barlaud, "Tow deterministic half-quadratic regularizition algorithems for computed imaging," in *IEEE Int. Conf. Image Processing*, vol. 2, 1994, pp. 168–172.

[73] F. Catte, P. Lions, J. M. Morel, and T. Coll, "Image selective smoothing and edge detection by nonlinear diffusion," *SIAM J. Numer. Anal.*, vol. 29, no. 1, pp. 182 –193, 1992.

[74] G. Gilboa, N. A. Sochen, and Y. Y. Zeevi, "Forward-and-backward diffusion processes for adaptive image enhancement and denoising," *IEEE Transactions on Image Processing*, vol. 11, no. 7, pp. 689–703, July 2002.

[75] L. Alvarez, F. Guichard, P.-L. Lions, and J.-M. Morel, "Axioms and fundamental equations of image processing," *Archive for Rational Mechanics and Analysis*, vol. 123, no. 3, pp. 199 – 257, 1993.

[76] D. Gabor, "Information theory in electron microscopy," *Laboratory Investigation*, vol. 14, pp. 801–807, June 1965.

[77] S. Osher and J. A. Sethian, "Fronts propagating with curvature-dependent speed: Algorithms based on Hamilton-Jacobi formulations," *Journal of Computational Physics*, vol. 79, pp. 12–49, 1988.

[78] L. Alvarez, P.-L. Lions, and J.-M. Morel, "Image selective smoothing and edge detection by nonlinear diffusion II," *SIAM Journal on Numerical Analysis*, vol. 29, no. 3, pp. 845–866, June 1992.

[79] G. Sapiro, "Vector (self) snakes: a geometric framework for color, texture, and multiscale image segmentation," in *Proceedings of IEEE International Conference on Image Processing (ICIP)*, vol. 1, Sept. 1996, pp. 817 – 820.

[80] J. Weickert, "Coherence-enhancing diffusion filtering," *International Journal of Computer Vision*, vol. 31, no. 2, pp. 111 – 127, 1999.

[81] D. Tschumperle and R. Deriche, "Vector-valued image regularization with PDE's: a common framework for different applications," *IEEE Transactions on Pattern Analysis and Machine Intelligence*, vol. 27, no. 4, pp. 506–517, Apr. 2005.

[82] D. Tschumperle, "Fast anisotropic smoothing of multi-valued images using curvature-preserving PDE's," *International Journal of Computer Vision*, vol. 68, no. 1, pp. 65 – 82, June 2006.

[83] R. A. Carmona and S. Zhong, "Adaptive smoothing respecting feature directions," *IEEE Transactions on Image Processing*, vol. 7, no. 3, pp. 353 – 358, March 1998.

[84] F. Voci, S. Eiho, N. Sugimoto, and H. Sekibuchi, "Estimating the gradient threshold in the Perona-Malik equation," *IEEE Signal Processing Magazine*, vol. 21, no. 3, pp. 39 –65, May 2004. [Online]. Available: http://dx.doi.org/10.1109/MSP.2004.1296541

[85] H. Yu and C.-S. Chua, "GVF-based anisotropic diffusion models," *IEEE Transaction on image processing*, vol. 15, no. 6, pp. 1517–1524, June 2006.

[86] M. Bertalmio, P. Fort, and D. Sanchez-Crespo, "Real-time, accurate depth of field using anisotropic diffusion and programmable graphics cards," 2004, pp. 767–773.

[87] P. Mrazek and J. Weickert, "From two-dimensional nonlinear diffusion to coupled Haar wavelet shrinkage," *Visual Communication and Image Representation*, vol. 18, no. 2, pp. 162–175, Jan. 2007.

[88] A. Rosenfeld and A. C. Kak, *Digital Image Processing*, 2nd ed. New York: Academic Press, 1982, vol. 2.

[89] M. Hajiaboli, M. O. Ahmad, and C. Wang, "An edge adapting Laplacian kernel for nonlinear diffusion filters," *IEEE Transactions on Image Processing*, 2011. [Online]. Available: http://dx.doi.org/10.1109/TIP.2011.2172803

[90] J. S. J. Lee, R. M. Haralick, and L. G. Shapiro, "Morphologic edge detection," *IEEE Journal of Robotics and Automation*, vol. 3, no. 2, pp. 142–156, Apr. 1987.

[91] J. Weickert and H. Scharr, "A scheme for coherence-enhancing diffusion filtering with optimized rotation invariance," *Journal of Visual Communication and Image Representation*, vol. 13, no. 1-2, pp. 103 – 118, March 2002. [Online]. Available: http://dx.doi.org/10.1006/jvci.2001.0495

[92] J. Immerkar, "Fast noise variance estimation," *Computer Vision and Image Understanding*, vol. 64, no. 2, pp. 300–302, Sept. 1996.

[93] T. Lindeberg, "Scale-space for discrete signals," *IEEE Trans. Pattern Anal. Mach. Intell.*, vol. 12, no. 3, pp. 234–254, March 1990.

[94] ——, "Discrete derivative approximations with scale-space properties: a basis for low-level feature extraction," *Journal of Mathematical Imaging and Vision*, vol. 3, no. 4, pp. 349 – 376, 1993.

[95] M. Welk, G. Gilboa, and J. Weickert, "Theoretical foundations for discrete forward-and-backward diffusion filtering," in *Scale Space and Variational Methods in Computer Vision*, 2009.

[96] G. Gilboa, Y. Zeevi, and N. Sochen, "Image enhancement segmentation and denoising by time dependent nonlinear diffusion processes," in *Proc. International Conference on Image Processing (ICIP)*, vol. 3, Oct. 2001, pp. 134 –137.

[97] R. C. Gonzalez and R. E. Woods, *Digital Image Processing.* Upper Saddle River, NJ: Prentice Hall, 2002.

[98] M. Hajiaboli, M. O. Ahmad, and C. Wang, "Nonlinear diffusion filtering for Poisson noise removal," *Submitted for publication to IEEE Transactions on Image Processing.*

[99] A. A. Samsonov and C. R. Johnson, "Noise-adaptive nonlinear diffusion filtering of MR images with spatially varying noise levels," *Magnetic Resonance in Medicine*, vol. 52, no. 4, pp. 798–806, Oct. 2004.

[100] D. Padfield and R. Manjeshwar, "Adaptive conductance filtering for spatially varying noise in PET images," in *Proc. SPIE*, vol. 6144, Feb. 2006, pp. 1 – 6. [Online]. Available: http://dx.doi.org/10.1117/12.654243

[101] T. Le, R. Chartrand, and T. J. Asaki, "A variational approach to reconstructing images corrupted by Poisson noise," *J. Math. Imaging Vis.*, vol. 27, no. 3, pp. 257–263, April 2007.

[102] J. G. Skellam, "The frequency distribution of the difference between two poisson variates belonging to different populations," *Journal of the Royal Statistical Society: Series A*, vol. 109, no. 3, p. 296, 1946.

[103] Y. Hwang, J.-S. Kim, and I.-S. Kweon, "Sensor noise modeling using the Skellam distribution: Application to the color edge detection," in *Proc. IEEE Conference on Computer Vision and Pattern Recognition.*, June 2007, pp. 1 –8.

[104] Z. Harmany, R. Marcia, and R. Willett, "This is SPIRAL-TAP: Sparse Poisson intensity reconstruction algorithms – theory and practice," *IEEE Transactions on Image Processing*, vol. 21, no. 3, pp. 1084–1096, March 2011.